Resistance of SARS-CoV-2 variants to neutralization by monoclonal and serum-derived polyclonal antibodies

Rita E. Chen[1,2,15], Xianwen Zhang[3,15], James Brett Case [1], Emma S. Winkler[1,2], Yang Liu[3], Laura A. VanBlargan[1], Jianying Liu[4,5], John M. Errico[2], Xuping Xie [3], Naveenchandra Suryadevara [6], Pavlo Gilchuk[6], Seth J. Zost [6], Stephen Tahan[7], Lindsay Droit[7], Jackson S. Turner[2], Wooseob Kim [2], Aaron J. Schmitz [2], Mahima Thapa[2], David Wang[7], Adrianus C. M. Boon[1,2,7], Rachel M. Presti [1], Jane A. O'Halloran[1], Alfred H. J. Kim [1], Parakkal Deepak [1], Dora Pinto[8], Daved H. Fremont[2,9], James E. Crowe Jr [6,10], Davide Corti[8], Herbert W. Virgin [2,11,12], Ali H. Ellebedy [2,7,13 ✉], Pei-Yong Shi [3,5,14 ✉] and Michael S. Diamond[1,2,7,13 ✉]

Severe acute respiratory syndrome coronavirus 2 (SARS-CoV-2) has caused the global COVID-19 pandemic. Rapidly spreading SARS-CoV-2 variants may jeopardize newly introduced antibody and vaccine countermeasures. Here, using monoclonal antibodies (mAbs), animal immune sera, human convalescent sera and human sera from recipients of the BNT162b2 mRNA vaccine, we report the impact on antibody neutralization of a panel of authentic SARS-CoV-2 variants including a B.1.1.7 isolate, chimeric strains with South African or Brazilian spike genes and isogenic recombinant viral variants. Many highly neutralizing mAbs engaging the receptor-binding domain or N-terminal domain and most convalescent sera and mRNA vaccine-induced immune sera showed reduced inhibitory activity against viruses containing an E484K spike mutation. As antibodies binding to spike receptor-binding domain and N-terminal domain demonstrate diminished neutralization potency in vitro against some emerging variants, updated mAb cocktails targeting highly conserved regions, enhancement of mAb potency or adjustments to the spike sequences of vaccines may be needed to prevent loss of protection in vivo.

Severe acute respiratory syndrome coronavirus 2 (SARS-CoV-2) has caused the global COVID-19 pandemic infecting more than 111 million people and causing 2.4 million deaths. Clinical disease in humans ranges from asymptomatic infection to pneumonia, severe respiratory compromise, multi-organ failure and systemic inflammatory syndromes. The rapid expansion and prolonged nature of the COVID-19 pandemic and its accompanying morbidity, mortality and destabilizing socioeconomic effects have made the development of SARS-CoV-2 therapeutics and vaccines an urgent global health priority[1]. Indeed, the emergency use authorization and rapid deployment of antibody-based countermeasures, including mAbs, immune plasma therapy and messenger RNA, and inactivated and viral-vectored vaccines has provided hope for curtailing disease and ending the pandemic.

The spike protein of the SARS-CoV-2 virion binds the cell-surface receptor angiotensin-converting enzyme 2 (ACE2) to promote entry into human cells[2]. Because the spike protein is critical for viral entry,

it has been targeted for vaccine development and therapeutic antibody interventions. SARS-CoV-2 S proteins are cleaved to yield S1 and S2 fragments. The S1 protein includes the N-terminal (NTD) and receptor-binding (RBD) domains, whereas the S2 protein promotes membrane fusion. The RBD is recognized by many potently neutralizing monoclonal antibodies[3–7], protein-based inhibitors[8] and serum antibodies[9].

The current suite of antibody therapeutics and vaccines was designed with a spike protein based on strains circulating during the early phases of the pandemic in 2020. More recently, variants with enhanced transmissibility have emerged in the United Kingdom (B.1.1.7), South Africa (B.1.351), Brazil (B.1.1.248) and elsewhere with multiple substitutions in the spike protein, including in the NTD and the receptor-binding motif (RBM) of the RBD. Preliminary studies with pseudoviruses suggest that neutralization by some antibodies and immune sera may be diminished against variants expressing mutations in the spike gene[10–13]. Given these

[1]Department of Medicine, Washington University School of Medicine, St. Louis, MO, USA. [2]Department of Pathology & Immunology, Washington University School of Medicine, St. Louis, MO, USA. [3]Department of Biochemistry and Molecular Biology, University of Texas Medical Branch, Galveston, TX, USA. [4]Departments of Microbiology and Immunology, University of Texas Medical Branch, Galveston, TX, USA. [5]Institute for Human Infections and Immunity, University of Texas Medical Branch, Galveston, TX, USA. [6]Vanderbilt Vaccine Center, Vanderbilt University Medical Center, Nashville, TN, USA. [7]Department of Molecular Microbiology, Washington University School of Medicine, St. Louis, MO, USA. [8]Humabs BioMed SA, a subsidary of Vir Biotechnology, Bellinzona, Switzerland. [9]Department of Biochemistry and Molecular Biophysics, Washington University School of Medicine, St. Louis, MO, USA. [10]Departments of Pediatrics and Pathology, Microbiology and Immunology, Vanderbilt University Medical Center, Nashville, TN, USA. [11]Vir Biotechnology, San Francisco, CA, USA. [12]University of Texas Southwestern Medical Center, Dallas, TX, USA. [13]Andrew M. and Jane M. Bursky Center for Human Immunology and Immunotherapy Programs, Washington University School of Medicine, Saint Louis, MO, USA. [14]Sealy Institute for Vaccine Sciences, University of Texas Medical Branch, Galveston, TX, USA. [15]These authors contributed equally: Rita E. Chen, Xianwen Zhang. ✉e-mail: ellebedy@wustl.edu; peshi@utmb.edu; diamond@wusm.wustl.edu

concerns, here, we evaluated the neutralizing activity in cell culture of monoclonal and serum-derived polyclonal antibodies against a panel of authentic, infectious SARS-CoV-2 variants, including a B.1.1.7 isolate, chimeric Washington strains with a South African (Wash SA-B.1.351) or Brazilian (Wash BR-B.1.1.248) spike gene and isogenic recombinant variants with designed mutations or deletions at positions 69-70, 417, 484, 501, 614 and/or 681 of the spike protein. Our data show moderate to substantially diminished neutralizing potency of antibodies and sera against chimeric SARS-CoV-2 strains or isogenic variants containing a mutation at position 484.

Results

To evaluate the effects of SARS-CoV-2 strain variation on antibody neutralization, we obtained or generated a panel of authentic infectious SARS-CoV-2 strains with sequence variations in the spike gene (Fig. 1a–c). A B.1.1.7 isolate had signature changes in the spike gene[14], including the 69–70 and 144–145 deletions and N501Y, A570D, D614G and P681H substitutions. We created a chimeric, fully infectious SARS-CoV-2 with a South African spike gene (Wash SA-B.1.351; D80A, 242-244 deletion, R246I, K417N, E484K, N501Y, D614G and A701V) and a panel of isogenic spike mutants (D614G, K417N/D614G, E484K/D614G, N501Y/D614G, P681H/D614G, del69-70/N501Y/D614G, E484K/N501Y/D614G and K417N/E484K/N501Y/D614G) in the Washington strain background (2019n-CoV/USA_WA1/2020 (WA1/2020)). Recombinant viruses and B.1.1.7 were propagated in Vero-TMPRSS2 and Vero-hACE2-TMPRSS2 cells expressing transmembrane protease serine 2 (TMPRSS2) and human ACE2 (hACE2) to prevent the development of adventitious mutations in the spike, especially at or near the furin cleavage site, which accumulate rapidly in Vero E6 cells[15] and can impact entry pathways and virulence[16]. All viruses were used at low passage (p0 or p1) and deep sequenced to confirm the presence of expected mutations and an absence of cell type-dependent adaptations (Supplementary Table 1).

We tested our panel of viruses for antibody-mediated neutralization in Vero-hACE2-TMPRSS2 cells and then repeated some experiments with Vero-TMPRSS2 cells to evaluate for effects of hACE2 over-expression on neutralization[17]. We performed high-throughput focus reduction neutralization tests (FRNTs)[18] using a panel of neutralizing mAbs recognizing distinct and overlapping epitopes in the RBD, including some having potential use in humans. Class 1 antibodies (such as COV2-2196, COV2-2072, COV2-2050, COV2-2381, COV2-2130, COVOX-384, COVOX-40, 1B07, S2E12, S2H58 and S2X259) are potently neutralizing, block soluble hACE2 binding and bind multiple proximal sites in the RBM of the RBD as determined by structural or escape mutation analyses (Extended Data Fig. 1a)[5,7,19,20]; class 2 neutralizing antibodies (such as S309, SARS2-3, SARS2-10, SARS2-31, SARS2-44) often cross-react with SARS-CoV, bind the base of the RBD (Extended Data Fig. 1b) and variably block hACE2 binding[3] (VanBlargan and Diamond, unpublished results); and class 3 neutralizing mAbs (such as COV2-2676 and COV2-2489) recognize the NTD (Extended Data Fig. 1c)[21].

Initially, we performed neutralization tests with WA1/2020 D614G and the two Vero cell types (Fig. 1d–i and Extended Data Fig. 2). With the D614G strain, neutralization by the majority of class 1 and class 2 mAbs was similar in Vero-hACE2-TMPRSS2 and Vero-TMPRSS2 cells. However, NTD-reactive mAbs showed greater potency (up to 13-fold) and more complete neutralization on Vero-TMPRSS2 than Vero-hACE2-TMPRSS2 cells (Fig. 1f). Given that the expression of hACE2 on recipient Vero cells can impact the neutralizing activity of mAbs binding outside of the RBD, we performed subsequent studies with both cell types.
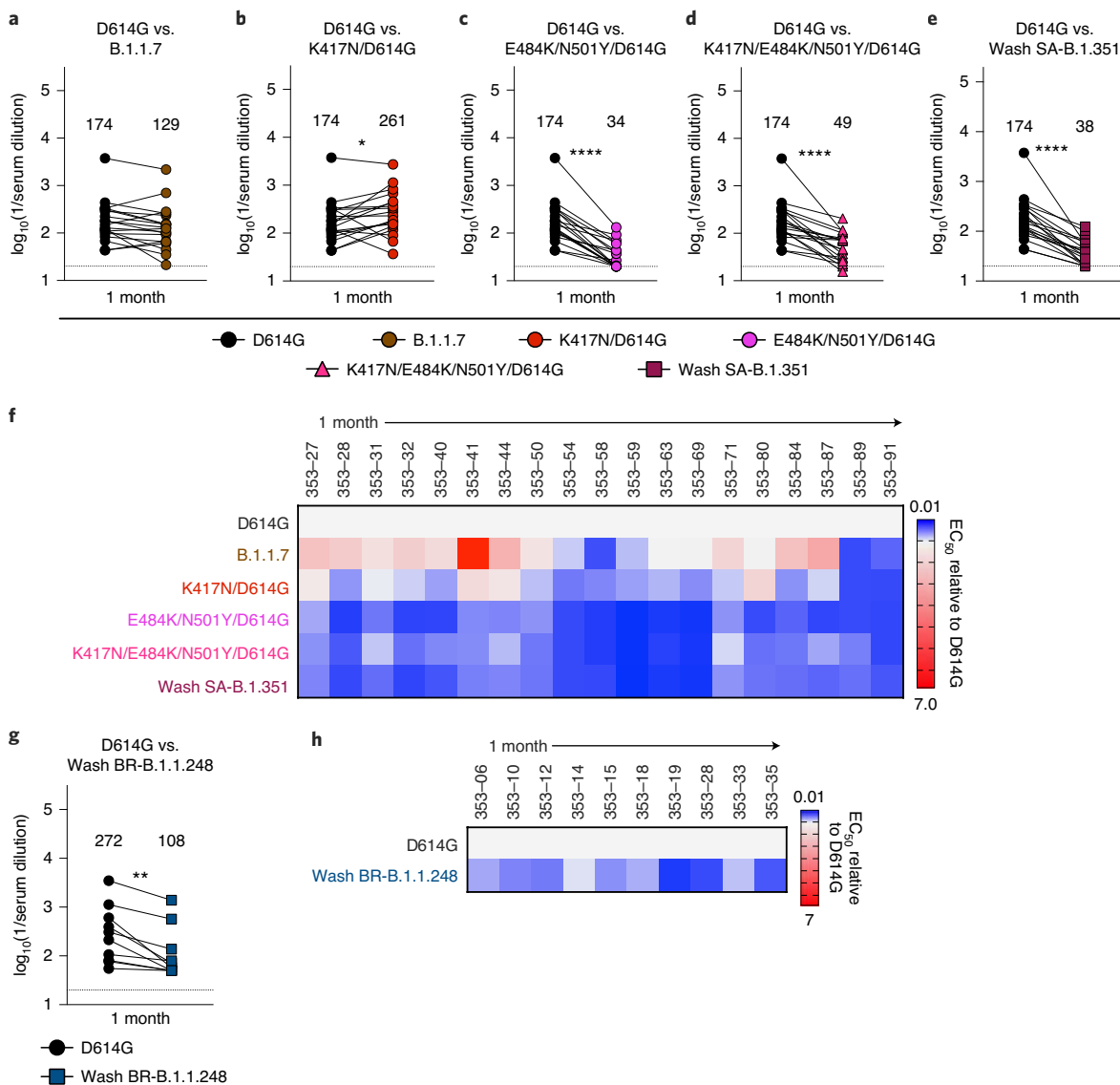
We next assessed the impact of spike protein mutations on mAb neutralization in Vero-hACE2-TMPRSS2 cells (Fig. 1h) and Vero-TMPRSS2 cells (Fig. 1i). We observed the following patterns with the variant viruses: (1) The P681H mutation (in the C-terminal region of S1) and the 69–70 deletion (in the NTD) had marginal effects on neutralization potency of the RBM and RBD mAbs we evaluated. It was difficult to assess the impact of the P681H and other mutations on the NTD mAbs, as these mAbs neutralized the D614G virus poorly at baseline in Vero-hACE2-TMPRSS2 cells; (2) The K417N mutation resulted in ~27-fold reduction in neutralization by mAb COVOX-40 but did not negatively affect other mAbs in our panel. If anything, several class 1 mAbs and also SARS2-44 showed slightly improved inhibitory activity ($P = 0.002$, two-tailed Wilcoxon matched-pairs signed-rank test) with this mutation; (3) Mutation at N501Y reduced the neutralizing activity of COVOX-40, SARS2-31 and SARS2-10 slightly but did not alter the potency of other mAbs substantively; this result is consistent with data showing that human convalescent sera efficiently neutralize viruses with N501Y substitutions[22–24]; (4) The E484K mutation negatively impacted the potency of several class 1 antibodies. Compared to the D614G virus, mAbs COV2-2196, COV2-3025, COV2-2381 and S2E12 showed four to fivefold reduced activity against the E484K virus and COV2-2050, 1B07, COVOX-384 and S2H58 lost virtually all neutralizing potential; (5) The combination of E484K and N501Y mutations, which is present in the circulating South African B.1.351 and Brazilian B.1.1.248 strains, showed even greater effects (6- to 13-fold reductions) on the activity of class 1 mAbs COV2-2196, COV2-3025, COV2-2381 and S2E12 mAbs; (6) When we tested class 1 mAbs for inhibition of the Wash SA-B.1.351 virus containing the full South African spike sequence, as expected, several mAbs (COV2-2050, 1B07, COVOX-384 and S2H58) lost activity in both Vero-hACE2-TMPRSS2 and Vero-TMPRSS2 cells. However, the reductions in neutralizing potential by other class 1 mAbs (COV2-2196, COV2-3025, COV2-2381 and S2E12) seen against the E484K/N501Y virus were absent with Wash SA-B.1.351, which contains additional mutations. The K417N substitution, which is located at the edge of the RBM (Fig. 1b) and enhances neutralization by some class 1 mAbs, may compensate for the negative effects on inhibition of the E484K/N501Y mutations. In comparison, we observed a distinct neutralization pattern with Wash SA-B.1.351 for class 2 and 3 mAbs. Because some mAbs neutralized poorly in Vero-hACE2-TMPRSS2 cells, we performed parallel experiments in Vero-TMPRSS2 cells. Class 2 mAbs binding the base of the RBD showed no substantive loss in potency against the Wash SA-B.1.351. However, the two NTD mAbs in class 3 (COV2-2676 and COV2-2489) lost neutralizing activity against Wash SA-B.1.351 in Vero-hACE2-TMPRSS2 and Vero-TMPRSS2 cells, consistent with recent data with other NTD mAbs and pseudoviruses[13]; (7) None of the class 1 mAbs lost neutralizing activity against the B.1.1.7 virus on Vero-hACE2-TMPRSS2 cells. Nonetheless, we observed some small reductions in potency (2.5- to 6-fold) with mAbs COV2-2381, S2E12 and S2X259 on Vero-TMPRSS2 cells, although they remained highly neutralizing. In comparison, we observed diminished (6- to 13-fold) neutralizing activity of some class 2 mAbs (SARS2-31 and S309) against the B.1.1.7 strain in Vero-hACE2-TMPRSS2 but not Vero-TMPRSS2 cells. The reduced potency of S309 mAb against B.1.1.7 strain in Vero-hACE2-TMPRSS2 cells contrasts with data showing that it binds avidly to the B.1.1.7 spike protein on the surface of cells and potently neutralizes a vesicular stomatitis virus (VSV) pseudotyped with B.1.1.7 spike protein in Vero E6 cells or a WA1/2020 virus derived in Vero CCL81 cells and tested on Vero-hACE2-TMPRSS2 or Vero-TMPRSS2 cells (Extended Data Fig. 3a–c). Finally, one of the NTD class 3 mAbs (COV2-2489) lost inhibitory activity against the B.1.1.7 strain in both cell types, possibly due to the deletions present in the NTD (69–70 and 144–145)[21].

Several academic and industry groups have developed mAb cocktails to overcome possible emergence of resistance during therapy[7,25]. We tested two mAb combinations that have potential use in humans (COV2-2196 + COV2-2130, Vanderbilt University Medical Center (with engineered derivatives being tested in clinical
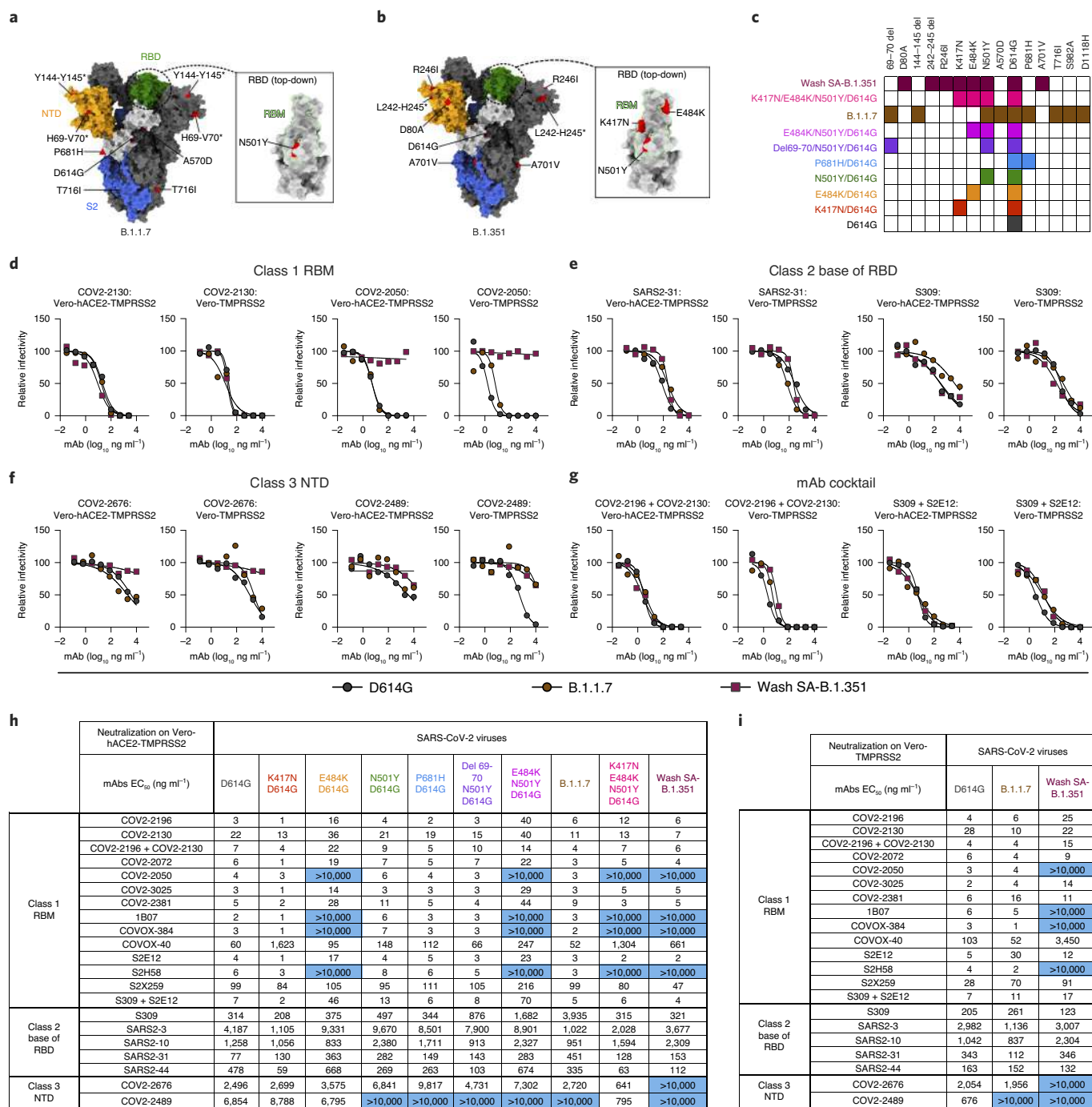
Fig. 1 | Neutralization of SARS-CoV-2 viral variants by mAbs. a,b, SARS-CoV-2 spike trimer. One protomer is highlighted, showing the NTD in orange, RBD in green and S2 portion of the molecule in blue, with N- and C-termini annotated. Substitutions in the B.1.1.7 variant (69–70 deletion, 144–145 deletion, A570D, D614G, P681H and T716I) are shaded in red (**a**). Red triangle depicts approximate location of P681H, which was not included in the model. Inset shows a top-down view of the RBD showing the location of the N501Y mutation contextualized with the RBM. Substitutions in the Wash SA-B.1.135 variant (242–244 deletion, D80A, R246I, D614G and A701V) are shaded in red (**b**). The red diamond denotes approximate location of D80A, which is buried in this view. Inset shows top-down view of the RBD with Wash SA-B.1.351 substitutions K417N, E484K and N501Y shaded red and contextualized with the RBM. For all panels, structures depicting spike protein were modeled using PDB: 7C2L. Structures depicting RBD were modeled using PDB: 6W41. All analyses and figures were generated with UCSF ChimeraX[49]. **c,** Viruses with indicated spike mutations. **d–f,** Neutralization curves in Vero-hACE2-TMPRSS2 cells (left) or Vero-TMPRSS2 cells (right) comparing the sensitivity of SARS-CoV-2 strains with class 1 (COV2-2130 and COV-2150) (**d**), class 2 (SARS2-31 and S309) (**e**) and class 3 (COV2-2676 and COV2-2489) (**f**) mAbs and indicated viruses. **g,** Also shown are the neutralization curves for antibody cocktails (COV2-2196 + COV2-2130 and S309 + S2E12). One representative experiment of two performed in technical duplicate is shown. **h,i,** Summary of EC$_{50}$ values (ng ml^{-1}) of neutralization of SARS-CoV-2 viruses propagated on the indicated cells and performed in Vero-hACE2-TMPRSS2 (**h**) or Vero-TMPRSS2 (**i**) cells. Blue shading of cells shows virtually complete loss of neutralizing activity, EC$_{50}$ > 10,000 ng ml^{-1}.

h — Neutralization on Vero-hACE2-TMPRSS2 — SARS-CoV-2 viruses

	mAbs EC$_{50}$ (ng ml^{-1})	D614G	K417N D614G	E484K D614G	N501Y D614G	P681H D614G	Del 69-70 N501Y D614G	E484K N501Y D614G	B.1.1.7	K417N E484K N501Y D614G	Wash SA-B.1.351
Class 1 RBM	COV2-2196	3	1	16	4	2	3	40	6	12	6
	COV2-2130	22	13	36	21	19	15	40	11	13	7
	COV2-2196 + COV2-2130	7	4	22	9	5	10	14	4	7	6
	COV2-2072	6	1	19	7	5	7	22	3	5	4
	COV2-2050	4	3	>10,000	6	4	3	>10,000	3	>10,000	>10,000
	COV2-3025	3	1	14	3	3	3	29	3	5	5
	COV2-2381	5	2	28	11	5	4	44	9	3	5
	1B07	2	1	>10,000	6	3	3	>10,000	3	>10,000	>10,000
	COVOX-384	3	1	>10,000	7	3	3	>10,000	2	>10,000	>10,000
	COVOX-40	60	1,623	95	148	112	66	247	52	1,304	661
	S2E12	4	1	17	4	5	3	23	3	2	2
	S2H58	6	3	>10,000	8	6	5	>10,000	3	>10,000	>10,000
	S2X259	99	84	105	95	111	105	216	99	80	47
	S309 + S2E12	7	2	46	13	6	8	70	5	6	4
Class 2 base of RBD	S309	314	208	375	497	344	876	1,682	3,935	315	321
	SARS2-3	4,187	1,105	9,331	9,670	8,501	7,900	8,901	1,022	2,028	3,677
	SARS2-10	1,258	1,056	833	2,380	1,711	913	2,327	951	1,594	2,309
	SARS2-31	77	130	363	282	149	143	283	451	128	153
	SARS2-44	478	59	668	269	263	103	674	335	63	112
Class 3 NTD	COV2-2676	2,496	2,699	3,575	6,841	9,817	4,731	7,302	2,720	641	>10,000
	COV2-2489	6,854	8,788	6,795	>10,000	>10,000	>10,000	>10,000	>10,000	795	>10,000

i — Neutralization on Vero-TMPRSS2 — SARS-CoV-2 viruses

	mAbs EC$_{50}$ (ng ml^{-1})	D614G	B.1.1.7	Wash SA-B.1.351
Class 1 RBM	COV2-2196	4	6	25
	COV2-2130	28	10	22
	COV2-2196 + COV2-2130	4	4	15
	COV2-2072	6	4	9
	COV2-2050	3	4	>10,000
	COV2-3025	2	4	14
	COV2-2381	6	16	11
	1B07	6	5	>10,000
	COVOX-384	3	1	>10,000
	COVOX-40	103	52	3,450
	S2E12	5	30	12
	S2H58	4	2	>10,000
	S2X259	28	70	91
	S309 + S2E12	7	11	17
Class 2 base of RBD	S309	205	261	123
	SARS2-3	2,982	1,136	3,007
	SARS2-10	1,042	837	2,304
	SARS2-31	343	112	346
	SARS2-44	163	152	132
Class 3 NTD	COV2-2676	2,054	1,956	>10,000
	COV2-2489	676	>10,000	>10,000

Fig. 2 | Neutralization of SARS-CoV-2 viral variants by convalescent human serum in Vero-hACE2 TMPRSS2 cells. a–e, Paired analysis of neutralizing activity by convalescent human sera ($n = 19$) obtained approximately 1 month after mild SARS-CoV-2 infection against WA1/2020 D614G and variant viruses in Vero-hACE2-TMPRSS2 cells: B.1.1.7 (**a**), K417N/D614G (**b**), E484K/N501Y/D614G (**c**), K417N/E484K/N501Y/D614G (**d**) or Wash SA-B.1.351 (**e**). **g,** Paired analysis of neutralizing activity by a separate convalescent human sera cohort ($n = 10$) obtained approximately 1 month after mild SARS-CoV-2 infection against WA1/2020 D614G and Wash BR-B.1.1.248 in Vero-hACE2-TMPRSS2 cells. Results are from one experiment performed in duplicate (**a–e,g**). GMTs are shown above each graph. Dotted line represents the limit of detection of the assay. Two-tailed Wilcoxon matched-pairs signed-rank test: D614G versus B.1.1.7, $P = 0.0546$; D614G versus K417N/D614G, $P = 0.0361$; D614G versus E484K/N501Y/D614G, $P < 0.0001$; D614G versus K417N/E484K/N501Y/D614G, $P < 0.0001$; D614G versus Wash SA-B.1.351, $P < 0.0001$; D614G versus Wash BR-B.1.1.248, $P = 0.0020$. **f,h,** Heat maps of the relative neutralizing activity of sera from individual convalescent subjects against indicated SARS-CoV-2 viruses compared to recombinant WA1/2020 D614G. Blue, reduction; red, increase.

trials by AstraZeneca) and S309 + S2E12, Vir Biotechnology) for their inhibitory activity against the SARS-CoV-2 variant viruses (Fig. 1g–i). The COV2-2196 + COV2-2130 combination generally retained inhibitory activity (<fourfold reduction) against all strains. Although the S309 + S2E12 combination showed reduced (~tenfold) potency against the E484K/N501Y/D614G strain, it performed effectively against the Wash SA-B.1.351 virus, again suggesting that additional mutations in natural variants (such as K417N) enable some antibodies to function better against viruses containing E484K and N501Y mutations.

We next assessed how spike protein mutations impacted the neutralizing activity of polyclonal sera obtained from individuals ($n = 19$), approximately 1 month after mild SARS-CoV-2

infection[26]. Based on experiments with the mAbs, we used Vero-hACE2-TMPRSS2 cells and focused our testing on WA1/2020 D614G, B.1.1.7, Wash SA-B.1.351 and WA1/2020 D614G with mutations at K417N, E484K/N501Y or K417N/E484K/N501Y (Fig. 2 and Extended Data Fig. 4). When compared to the WA1/2020 D614G virus, we observed the following: (1) differences in neutralization were not observed with the B.1.1.7 strain (Fig. 2a); (2) a small increase (1.5-fold, $P < 0.05$) in neutralization was detected with the K417N virus (Fig. 2b), similar to that seen with some mAbs (Fig. 1h); and (3) serum neutralization titers were lower against E484K/N501Y (fivefold, $P < 0.0001$), K417N/E484K/N501Y (3.5-fold, $P < 0.0001$) and Wash SA-B.1.351 (4.6-fold, $P < 0.0001$) viruses (Fig. 2c–e), all of which contain the E484K mutation.

A heat map analysis showed that most individuals lost neutralizing activity against all three viruses containing the E484K and N501Y mutations (Fig. 2f). Given these results with viruses encoding E484K mutations, we performed separate studies with human convalescent serum (n = 10) and a chimeric SARS-CoV-2 WA1/2020 strain encoding a Brazilian variant spike gene (Wash BR-B.1.1.248; L18F, T20N, P26S, D138Y, R190S, K417T, E484K, N501Y, D614G, H655Y, T1027I and V1176F; Extended Data Fig. 5a). As expected, several class 1 (RBM-binding) and class 3 (NTD-binding) mAbs showed reduced neutralizing activity against Wash BR-B.1.1.248 (Extended Data Fig. 5b,c). Nonetheless, we observed a smaller yet significant decrease (2.5-fold, $P < 0.01$) in neutralization potency of convalescent serum against Wash BR-B.1.1.248 (Fig. 2g,h and Extended Data Fig. 4).

Given that viruses containing changes at positions 484 and 501 escape neutralization by serum from convalescent humans, we next examined the effects of vaccine-induced antibody responses. Initially, we interrogated sera from mice (n = 10), hamsters (n = 8) and nonhuman primates (NHPs; rhesus macaques, n = 6) obtained 1 month after immunization with ChAd-SARS-CoV-2, a chimpanzee adenoviral vectored vaccine encoding for a prefusion stabilized form of the spike protein[27–29]. Using Vero-hACE2-TMPRSS2 cells, we assessed serum neutralization of WA1/2020 D614G, B.1.1.7, Wash SA-B.1.351 and recombinant WA1/2020 D614G viruses with mutations at K417N, E484K/N501Y or K417N/E484K/N501Y (Extended Data Fig. 6). For serum samples from mice, when comparing the geometric mean neutralization titers (GMTs) of neutralization to the WA1/2020 D614G strain, we observed a slight increase (1.9-fold, $P < 0.05$) with K417N (Fig. 3b), decreases with E484K/N501Y (ninefold, $P < 0.001$; Fig. 3c), K417N/E484K/N501Y (fivefold, $P < 0.01$; Fig. 3d) and Wash SA-B.1.351 (fivefold, $P < 0.01$; Fig. 3e), yet no significant differences with B.1.1.7. (Fig. 3a). In a heat map plot (Fig. 3p), nine of the ten mouse sera show a loss of neutralizing activity against multiple viruses containing the E484K mutation. In hamsters, the results were similar. We observed a marked decrease (10- to 12-fold, $P < 0.01$) in serum neutralization of E484K/N501Y, K417N/E484K/N501Y and Wash SA-B.1.351 (Fig. 3h–j). Statistically significant differences in neutralization were not observed with K417N and B.1.1.7 viruses (Fig. 3f,g). This pattern was reflected at the individual sample level (Fig. 3q). In NHPs, we also observed a substantial decrease (9- to 11-fold, $P < 0.05$) in serum neutralization of E484K/N501Y, K417N/E484K/N501Y and Wash SA-B.1.351 (Fig. 3m–o). In comparison, with B.1.1.7 (Fig. 3k) or K417N (Fig. 3l) viruses, we detected no change or small significant increases (1.5-fold, $P < 0.05$) in neutralization, respectively. The heat map analysis showed that all NHP sera consistently exhibited reduced neutralizing activity against viruses containing the E484K mutation (Fig. 3r).

Because samples from human immunization trials with ChAd-SARS-CoV-2 are not yet available, we interrogated sera from individuals who received the Pfizer-BioNTech (BNT162b2) vaccine, a lipid nanoparticle encapsulated-mRNA that encodes a similar membrane-bound, prefusion stabilized form of the full-length SARS-CoV-2 spike protein[30]. We tested sera (Extended Data Figs. 7 and 8) for neutralization of our panel of SARS-CoV-2 variants (Fig. 4a–f). Compared to the WA1/2020 D614G variant, we observed moderate reductions in neutralizing activity (GMTs) of B.1.1.7 (twofold, $P < 0.01$; Fig. 4a) and E484K/N501Y (fourfold, $P < 0.0001$; Fig. 4c) and larger decreases in activity against Wash SA-B.1.351 (tenfold, $P < 0.0001$; Fig. 4d), with all participants showing substantially reduced potency (Fig. 4f), results that agree with pseudovirus studies[13]. Analogous to the results with human convalescent sera (Fig. 2g), we observed a smaller decrease (2.2-fold, $P < 0.01$) in neutralization potency of serum from vaccine recipients against the Wash BR-B.1.1.248 virus (Fig. 4e). Significant differences in neutralizing activity were not detected with K417N/D614G (Fig. 4b).

Because of the differences in neutralization seen with some mAbs on Vero-hACE2-TMPRSS2 and Vero-TMPRSS2 cells (Fig. 1h,i), we also evaluated the impact of hACE2 receptor expression on neutralizing activity of serum samples from convalescent adults (Fig. 5a–d) and from BNT162b2 mRNA-vaccinated individuals (Fig. 5e–h). Given the limited remaining serum quantities, we performed neutralization experiments on Vero-TMPRSS2 cells with WA1/2020 D614G, B.1.1.7 and Wash SA-B.1.351 and Wash BR-B.1.1.248 viruses. These experiments (Extended Data Fig. 9) revealed the following: (1) Convalescent and vaccine sera showed small yet significant reductions (1.7- to 2.5-fold, $P < 0.01$) in neutralizing activity of B.1.1.7 compared to the WA1/2020 D614G virus (Fig. 5a,e). (2) Sera from both convalescent and vaccinated individuals showed a marked six- to ninefold reduction ($P < 0.01$) in neutralizing potency against the Wash SA-B.1.351 virus (Fig. 5b,f); and (3) we again observed a smaller decrease (1.7- to 4.5-fold, $P < 0.01$) in neutralization potency of serum against Wash BR-B.1.1.248, (Fig. 5c,g). The results were similar in magnitude between Vero-hACE2-TMPRSS2 and Vero-TMPRSS2 cells (see also Fig. 4a,d,e) and suggest that cellular expression of hACE2 does not markedly impact neutralization outcome of polyclonal antibodies in these assays.

Discussion

Our in vitro experiments using a B.1.1.7 isolate and engineered variants in the backbone of the WA1/2020 strain establish that mutations in the spike can impact the potency of antibody neutralization. Some neutralizing mAbs targeting the base of the RBD or NTD showed reduced activity against the B.1.1.7 isolate, whereas others targeting the RBM or NTD failed to inhibit infection of Wash SA-B.1.351, Wash BR-B.1.1.248 or variants containing the E484K mutation. These finding are potentially important because the RBM has functional plasticity[31,32] and additional mutations in this region that occur as the pandemic evolves could further impact the efficacy of mAb therapies or vaccines. Our results establishing the E484K substitution as a vulnerability for multiple neutralizing mAbs are consistent with deep mutational scanning or VSV-SARS-CoV-2-based neutralization escape screening campaigns[31,33]. However, several other highly neutralizing mAbs (such as COV2-2196,

Fig. 3 | Resistance of SARS-CoV-2 viral variants to neutralization by vaccine-induced serum derived from mice, hamsters and NHPs. a–o, Paired analysis of neutralizing activity by sera from mice (**a–e**, n = 10), hamsters (**f–j**, n = 8) and NHPs (**k–o**, n = 6) obtained ~30 d after a single intranasal immunization with an adenoviral vectored SARS-CoV-2 vaccine (ChAd-SARS-CoV-2-S[27]). Neutralization data on Vero-hACE2-TMPRSS2 cells is displayed as WA1/2020 D614G versus the variant viruses: B.1.1.7 (**a,f,k**), K417N/D614G (**b,g,l**), E484K/N501Y/D614G (**c,h,m**), K417N/E484K/N501Y/D614G (**d,i,n**) or Wash SA-B.1.351 (**e,j,o**). Results are from one experiment performed in duplicate, with some exceptions due to limited sample. GMT values are shown above each graph. Dotted line represents the limit of detection of the assay. Two-tailed Wilcoxon matched-pairs signed-rank test was used. Mouse sera: D614G versus B.1.1.7, $P = 0.323$; D614G versus K417N/D614G, $P = 0.0020$; D614G versus E484K/N501Y/D614G, $P = 0.0020$; D614G versus K417N/E484K/N501Y/ D614G, $P = 0.0039$; D614G versus Wash SA-B.1.351, $P = 0.0020$. Hamster sera: D614G versus B.1.1.7, $P = 0.9453$; D614G versus K417N/D614G, $P > 0.9999$; D614G versus E484K/N501Y/D614G, $P = 0.0078$; D614G versus K417N/E484K/N501Y/D614G, $P = 0.0078$; D614G versus Wash SA-B.1.351, $P = 0.0078$. NHP sera: D614G versus B.1.1.7, $P = 0.0625$; D614G versus K417N/D614G, $P = 0.0312$; D614G versus E484K/N501Y/D614G, $P = 0.0312$; D614G versus K417N/E484K/N501Y/D614G, $P = 0.0312$; D614G versus Wash SA-B.1.351, $P = 0.0312$. **p–r**, Heat maps of the relative neutralizing activity of sera from individual mice (**p**), hamsters (**q**) and NHPs (**r**) against indicated SARS-CoV-2 viruses compared to WA1/2020 D614G. Blue, reduction; red, increase.

COV2-2381, COV2-3025 and S2E12) showed intact or only mildly diminished inhibitory activity against the suite of variant viruses we tested, possibly because they bind the RBM at sites other than the E484K residue (Table 1). Moreover, cocktails of mAbs binding different epitopes of the spike protein overcame virus resistance to individual mAbs. Alternative approaches to addressing the diminished mAb neutralization activity by variant SARS-CoV-2 lineages include targeting of conserved regions of the spike and identifying
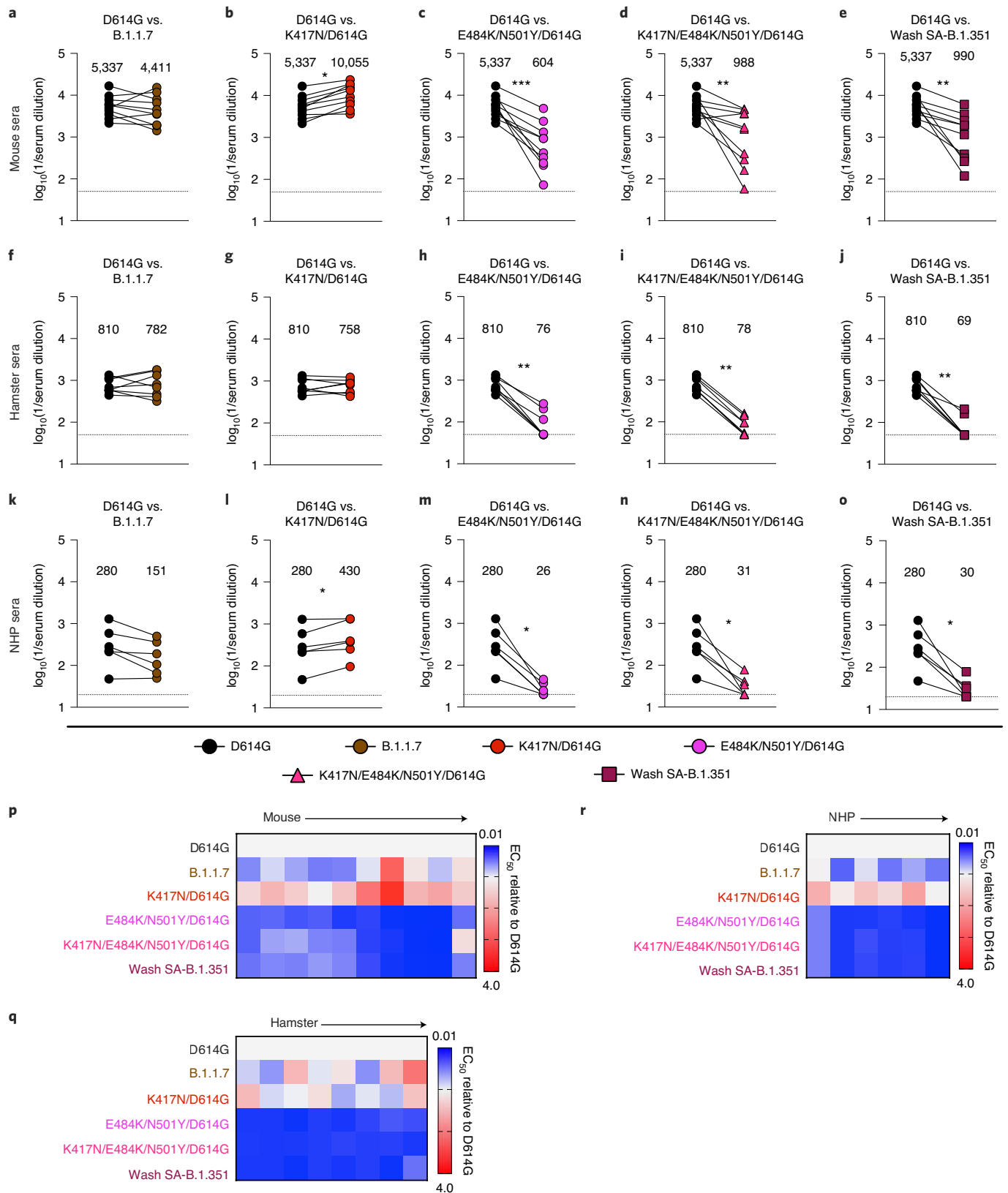
Table 1 | mAbs used in this study

	MAb	Region	Species	EC50 values (ng ml⁻¹)[a] D614G	EC50 values (ng ml⁻¹)[a] E484K/D614G	Block ACE2 binding	Contact residues within RBM[b]	Binding site residues, aa position	Functionally important residues[c]	Other mapping data	References
CLASS 1	COV2-2196	RBD - RBM	human	3	16	yes	yes	455–456, 475–479, 484–489, 493	F486A, N487A (LOB)	Not competitive with COV2-2130	5,19,46
	COV2-2130	RBD - RBM	human	22	36	yes	yes	345–346, 439–441, 443–447, 449–450, 452, 484, 490, 492–494	K444A, G447R (LOB); and R346I, K444R, K444E (NE)	Not competitive with COV2-2196	5,19,46
	COV2-2072	RBD - RBM	human	6	19	yes	yes	N/A	N/A	COV2-2196 competitive	5,19
	COV2-2050	RBD - RBM	human	4	>10,000	yes	yes	N/A	E484K (LOB and NE)	COV2-2196 and COV2-2130 competitive	5,19,31
	COV2-3025	RBD - RBM	human	3	14	yes	yes	N/A	N/A	COV2-2196 competitive	5,19
	COV2-2381	RBD - RBM	human	5	28	yes	yes	N/A	N/A	COV2-2196 competitive	5,19
	1B07	RBD - RBM	mouse-human chimera	2	>10,000	yes	yes	N/A	E484A/D/G/K, F486Y (NE)	N/A	20
	S2E12	RBD - RBM	human	4	17	yes	yes	455–458, 473–493	G476S, F486A (LOB)	N/A	7, Starr, Corti et al. unpublished
	COVOX-384	RBD - RBM	human	3	>10,000	yes	yes	455–456, 456, 482–486	N/A	N/A	47
	COVOX-40	RBD - RBM	human	60	95	yes	yes	417, 409, 505	N/A	N/A	47
	S2H58	RBD - RBM	human	6	>10,000	yes	yes	N/A	E484K, F490L, S494P (LOB)		Starr, Corti et al. unpublished
	S2X259	RBD	human	99	105	yes	no	N/A	G504D (LOB)		48
CLASS 2	S309	RBD- BASE	human	314	375	no	no	333–335,337, 339–341, 343, 346,354, 356–361, 440–441, 444,509	N/A	N/A	3
	SARS2-3	RBD- BASE	mouse	4,187	9,331	no	no	N/A	N/A	CR3022 competitive	VanBlargan and Diamond, unpublished
	SARS2-10	RBD- BASE	mouse	1,258	833	yes	no	N/A	N/A	CR3022 competitive	VanBlargan and Diamond, unpublished
	SARS2-31	RBD- BASE	mouse	130	282	yes	no	N/A	K378E/Q, R408K, G504D (NE)	CR3022 competitive	VanBlargan and Diamond, unpublished
	SARS2-44	RBD- BASE	mouse	59	269	yes	no	N/A	N/A	CR3022 competitive	VanBlargan and Diamond, unpublished
CLASS 3	COV2-2676	NTD	human	2,496	3,575	no	no	N/A	Y144A, N164A (LOB) and F140S (NE)	COV2-2489 competitive	5,19,21
	COV2-2489	NTD	human	6,854	6,795	no	no	N/A	G142A, Y144A, F157A, N164A (LOB); and G142D, R158S (NE)	COV2-2676 competitive	5,19,21

[a]Neutralization potency determined by FRNT assay in Vero-hACE2-TMPRSS2 cells from Fig. 1 with D614G and E484K/D614G isolates. [b]Identified as engaging residues within the RBM site by direct binding ELISA or by epitope mapping using LOB assays. [c]LOB to spike protein; NE mutants assessed with SARS-CoV-2 WA1/2020. LOB, loss of binding; NE neutralization escape; N/A, data not available; EC50, half maximal effective concentration.
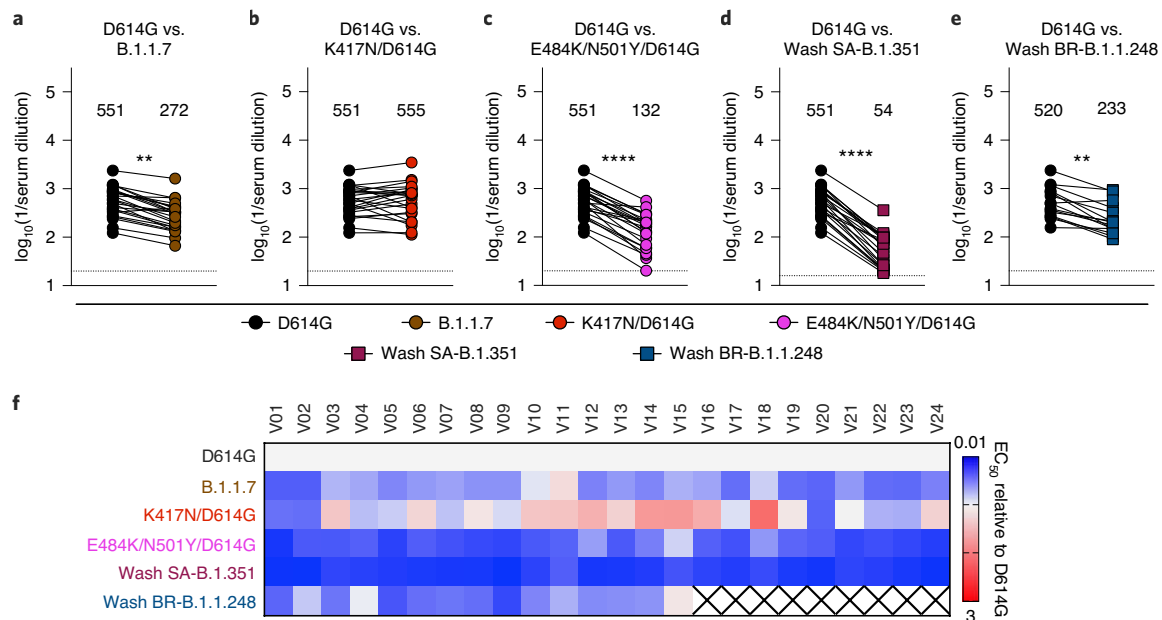
Fig. 4 | Resistance of SARS-CoV-2 viral variants to neutralization by human serum from Pfizer-BioNTech BNT162b2 mRNA-vaccinated individuals in Vero-hACE2-TMPRSS2 cells. Paired analysis of neutralizing activity by sera from humans ($n=24$) obtained after boosting with the BNT162b2 mRNA vaccine. **a**–**e**, Neutralization data on Vero-hACE2-TMPRSS2 cells is displayed with WA1/2020 D614G versus the variant viruses: B.1.1.7 (**a**), K417N/D614G (**b**), E484K/N501Y/D614G (**c**), Wash SA-B.1.351 (**d**) or Wash BR-B.1.1.248 (**e**) ($n=15$). Results are from one experiment performed in duplicate. GMT values are shown above each graph. Dotted line represents the limit of detection of the assay. Two-tailed Wilcoxon matched-pairs signed-rank test: D614G versus B.1.1.7, $P<0.0001$; D614G versus K417N/D614G, $P=0.6231$; D614G versus E484K/N501Y/D614G, $P<0.0001$; D614G versus K417N/E484K/N501Y/D614G, $P=0.8774$; D614G versus Wash SA-B.1.351, $P<0.0001$; D614G versus Wash BR-B.1.1.248, $P=0.0020$. **f**, Heat map of the relative neutralizing activity of sera from vaccinated individuals against indicated SARS-CoV-2 viruses compared to WA1/2020 D614G. Blue, reduction; red, increase. An X indicates sera was not evaluated.

clonal mAb variants with greater potency, such that a given dose of mAb can protect against a range of variants despite some decrease in neutralization activity.

Our studies with human sera from convalescent patients and recipients of the BNT162b2 mRNA vaccine and animal sera after immunization with a vaccine encoding a similar spike gene, demonstrate a lower potency of neutralization against E484K and N501Y-containing viruses (we did not perform studies with single-mutation viruses due to limited serum availability). This observation is unexpected given that antibody responses in animals and humans are polyclonal and in theory, should overcome resistance associated with individual mutations and loss of activity of particular B cell clones.

Our analyses agree with some studies showing substantial or complete escape against spike proteins corresponding to the South African lineage (B.1.351 or 501Y.V2) by antibodies in convalescent or vaccine-immune plasma using lentiviral-based pseudotype neutralization assays[10,11,23]. Moreover, they are consistent with studies showing loss of neutralization potency of human convalescent serum against VSV-SARS-CoV-2 chimeric virus variants containing the E484K mutation[34] and selection of escape E484K mutants under serial passage of convalescent COVID-19 plasma[35]. Indeed, similar findings with authentic SARS-CoV-2 viruses encoding E484K mutations were recently reported[36]. One unique trend we noticed was that convalescent and vaccine-induced immune sera neutralized infection of the chimeric SARS-CoV-2 strains encoding the Brazilian spike (B.1.1.248) better than the South African spike (B.1.351) even though both viruses encoded E484 and N501 mutations. While follow-up corroborating studies are warranted, this result could be due to the distinct set of mutations and/or deletions in the NTD region or enhanced neutralization of B.1.1.248 by

anti-RBD antibodies that bind outside of the RBM (Extended Data Fig. 5c). Overall, our findings may have therapeutic implications, as immune plasma derived from individuals infected early during the pandemic might fail to protect patients infected with more recent isolates containing the E484K mutation.

Limitations of the study. These studies focused exclusively on the impact of sequence changes in the spike protein on antibody neutralization in cell culture. Despite observing differences in serum neutralizing activity against authentic SARS-CoV-2 variant viruses, it remains unclear how this finding translates into effects on protection in the context of secondary infection or infection after vaccination with platforms using historical spike gene sequences. Although serum neutralizing titers are an anticipated correlate of protection[37], this measurement does not account for Fc effector functions; Fcγ receptor or complement protein engagement by non, weakly, or strongly neutralizing antibodies that bind the SARS-CoV-2 spike protein on the surface of infected cells could confer substantial protection[38–40]. Also, the role of memory T or B cells in protection against variant viruses is unknown and could prevent severe infection even in the setting of compromised serum antibody responses[41–43].

Moreover, the field still does not know whether Vero or other cell-based neutralization assays predict antibody-mediated protection. Indeed, primary cells targeted by SARS-CoV-2 in vivo can express unique sets of attachment and entry factors[44], which could impact receptor and entry blockade by specific antibodies. We observed that the cell line used can affect the potency of antibody neutralization against different SARS-CoV-2 variants. Such results may impact the congruity of data across laboratories and interpretation of effects of viral variants on vaccine efficacy. As an example, recent studies with Vero E6 cell-derived SARS-CoV-2 with spike
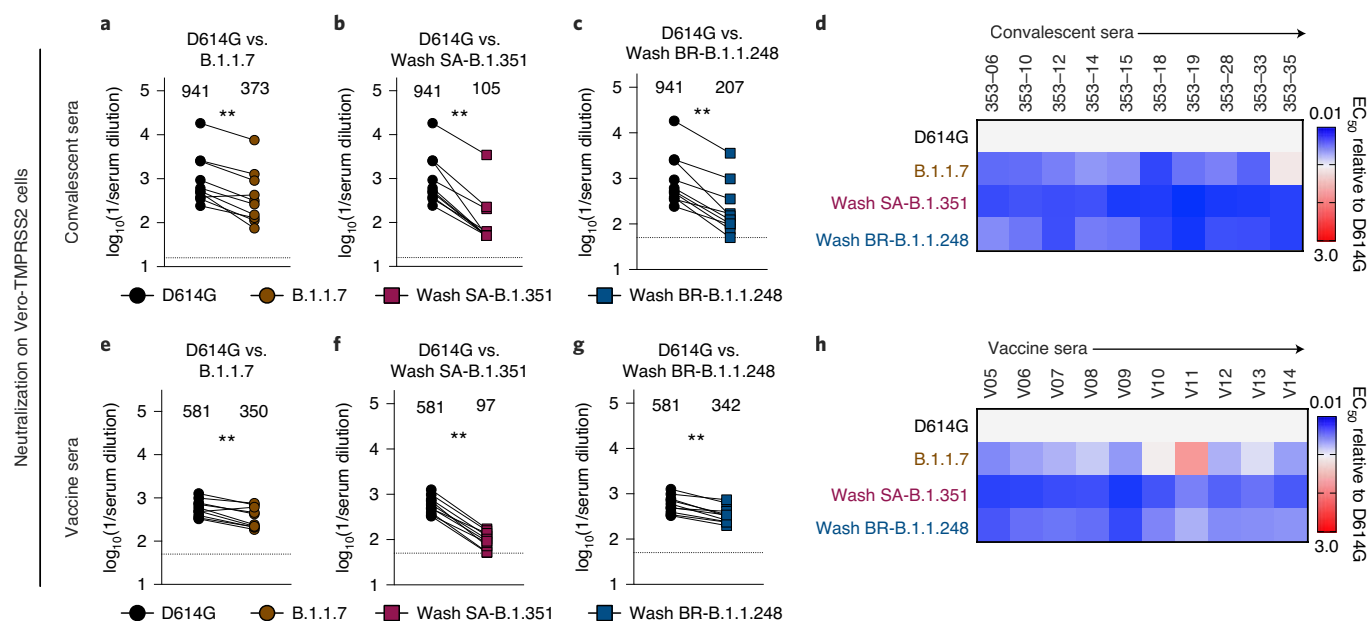
Fig. 5 | Resistance of SARS-CoV-2 viral variants to neutralization by human serum from convalescent and vaccinated individuals in Vero-TMPRSS2 cells. a–g, Sera from individuals who had been infected with SARS-CoV-2 (a–c, n = 10, ~1 month after infection) or vaccinated with the Pfizer-BioNTech mRNA vaccine (d–f, n = 10) were tested for neutralization of the indicated SARS-CoV-2 strains (WA1/2020 D614G (a–c,e–g), B.1.1.7 (a,e), Wash SA-B.1.351 (b,f), or Wash BR-B.1.1.248 (c,g) using a FRNT in Vero-TMPRSS2 cells. Results are from one experiment performed in duplicate, with some exceptions due to limited sample. GMT values are shown above each graph. Dotted line represents the limit of detection of the assay. Two-tailed Wilcoxon matched-pairs signed-rank test. Convalescent sera: D614G versus B.1.1.7, P = 0.0039; D614G versus Wash SA-B.1.351, P = 0.0020; D614G versus Wash BR-B.1.1.248, P = 0.0020. Vaccine sera: D614G versus B.1.1.7, P = 0.0039; D614G versus Wash SA-B.1.351, P = 0.0020; D614G versus Wash BR-B.1.1.248, P = 0.0020. h, Heat maps of the relative neutralizing activity of sera from convalescent (d) or vaccinated (h) individuals against indicated SARS-CoV-2 viruses compared to WA1/2020. Blue, reduction; red, increase.

proteins containing some (E484K, N501Y and D614G) or all of the South African mutations showed smaller 1.2 to 2.7-fold decreases in neutralization potency by BNT162b2 mRNA vaccine-elicited human immune sera[22,45]. When we compared neutralization of deep-sequenced confirmed p0 (Vero E6 cell-produced) and p1 (Vero-hACE2-TMPRSS2 cell-produced) K417N/E484K/N501Y/D614G viruses by immune serum from vaccinated animals or humans or naturally infected humans in the same recipient Vero-hACE2-TMPRSS2 cells, the viruses produced in Vero E6 cells were neutralized more efficiently (two- to threefold, P < 0.05) than those propagated in Vero-hACE2-TMPRSS2 cells (Extended Data Fig. 10). We speculate that TMPRSS2 might modify the spike protein of authentic SARS-CoV-2 in the producer cell such that some classes of antibodies no longer efficiently block infection of the recipient cell.

While our analysis of neutralizing antibody responses with authentic infectious SARS-CoV-2 variants on Vero-hACE2-TMPRSS2 and Vero-TMPRSS2 cells suggests that adjustments to some therapeutic antibody cocktails or existing spike sequences in vaccines might be necessary, corroborating in vivo studies are needed. Sequential infection and/or vaccination/infection studies in animals and analysis of vaccine efficacy in the setting of new variant infections ultimately will determine the impact of emerging SARS-CoV-2 lineages, especially those containing E484K mutations.

Online content

Any methods, additional references, Nature Research reporting summaries, source data, extended data, supplementary information, acknowledgements, peer review information; details of author contributions and competing interests; and statements of data and code availability are available at https://doi.org/10.1038/s41591-021-01294-w.

References

1. Sempowski, G. D., Saunders, K. O., Acharya, P., Wiehe, K. J. & Haynes, B. F. Pandemic preparedness: Developing vaccines and therapeutic antibodies For COVID-19. *Cell* **181**, 1458–1463 (2020).
2. Letko, M., Marzi, A. & Munster, V. Functional assessment of cell entry and receptor usage for SARS-CoV-2 and other lineage B betacoronaviruses. *Nat. Microbiol.* **5**, 562–569 (2020).
3. Pinto, D. et al. Cross-neutralization of SARS-CoV-2 by a human monoclonal SARS-CoV antibody. *Nature* **583**, 290–295 (2020).
4. Cao, Y. et al. Potent neutralizing antibodies against SARS-CoV-2 identified by high-throughput single-cell sequencing of convalescent patients' B cells. *Cell* **182**, 73–84 (2020).
5. Zost, S. J. et al. Rapid isolation and profiling of a diverse panel of human monoclonal antibodies targeting the SARS-CoV-2 spike protein. *Nat. Med.* **26**, 1422–1427 (2020).
6. Barnes, C. O. et al. SARS-CoV-2 neutralizing antibody structures inform therapeutic strategies. *Nature* **588**, 682–687 (2020).
7. Tortorici, M. A. et al. Ultrapotent human antibodies protect against SARS-CoV-2 challenge via multiple mechanisms. *Science* **370**, 950–957 (2020).
8. Cao, L. et al. De novo design of picomolar SARS-CoV-2 miniprotein inhibitors. *Science* **370**, 426–431 (2020).
9. Rathe, J.A. et al. SARS-CoV-2 serologic assays in control and unknown populations demonstrate the necessity of virus neutralization testing. *J. Infect. Dis.* https://doi.org/10.1093/infdis/jiaa797 (2020).
10. Wibmer, C.K. et al. SARS-CoV-2 501Y.V2 escapes neutralization by South African COVID-19 donor plasma. Preprint at *bioRxiv* https://doi.org/10.1101/2021.01.18.427166 (2021).
11. Wang, Z. et al. mRNA vaccine-elicited antibodies to SARS-CoV-2 and circulating variants. *Nature* https://doi.org/10.1038/s41586-021-03324-6 (2021).
12. Tada, T. et al. Neutralization of viruses with European, South African, and United States SARS-CoV-2 variant spike proteins by convalescent sera and BNT162b2 mRNA vaccine-elicited antibodies. Preprint at *bioRxiv* https://doi.org/10.1101/2021.02.05.430003 (2021).

13. Wang, P. et al. Increased resistance of SARS-CoV-2 variants B.1.351 and B.1.1.7 to antibody neutralization. Preprint at *bioRxiv* https://doi.org/10.1101/2021.01.25.428137 (2021).

14. Leung, K., Shum, M.H., Leung, G.M., Lam, T.T. & Wu, J.T. Early transmissibility assessment of the N501Y mutant strains of SARS-CoV-2 in the United Kingdom, October to November 2020. *Euro Surveill.* https://doi.org/10.2807/1560-7917.ES.2020.26.1.2002106 (2021).

15. Klimstra, W. B. et al. SARS-CoV-2 growth, furin-cleavage-site adaptation and neutralization using serum from acutely infected hospitalized COVID-19 patients. *J. Gen. Virol.* 101, 1156–1169 (2020).

16. Johnson, B.A. et al. Loss of furin cleavage site attenuates SARS-CoV-2 pathogenesis. *Nature* https://doi.org/10.1038/s41586-021-03237-4 (2021).

17. Rappazzo, C.G. et al. Broad and potent activity against SARS-like viruses by an engineered human monoclonal antibody. *Science* https://doi.org/10.1126/science.abf4830 (2021).

18. Case, J. B. et al. Neutralizing antibody and soluble ACE2 inhibition of a replication-competent VSV-SARS-CoV-2 and a clinical isolate of SARS-CoV-2. *Cell Host Microbe* 28, 475–485 (2020).

19. Zost, S. J. et al. Potently neutralizing and protective human antibodies against SARS-CoV-2. *Nature* 584, 443–449 (2020).

20. Alsoussi, W.B. et al. A potently neutralizing antibody protects mice against SARS-CoV-2 infection. *J. Immunol.* https://doi.org/10.4049/jimmunol.2000583 (2020).

21. Suryadevara, N. et al. Neutralizing and protective human monoclonal antibodies recognizing the N-terminal domain of the SARS-CoV-2 spike protein. Preprint at *bioRxiv* https://doi.org/10.1101/2021.01.19.427324 (2021).

22. Xie, X. et al. Neutralization of SARS-CoV-2 spike 69/70 deletion, E484K and N501Y variants by BNT162b2 vaccine-elicited sera. *Nat. Med.* https://doi.org/10.1038/s41591-021-01270-4 (2021).

23. Wu, K. et al. mRNA-1273 vaccine induces neutralizing antibodies against spike mutants from global SARS-CoV-2 variants. Preprint at *bioRxiv* https://doi.org/10.1101/2021.01.25.427948 (2021).

24. Rathnasinghe, R. et al. The N501Y mutation in SARS-CoV-2 spike leads to morbidity in obese and aged mice and is neutralized by convalescent and post-vaccination human sera. Preprint at *medRxiv* https://doi.org/10.1101/2021.01.19.21249592 (2021).

25. Baum, A. et al. Antibody cocktail to SARS-CoV-2 spike protein prevents rapid mutational escape seen with individual antibodies. *Science* https://doi.org/10.1126/science.abd0831 (2020).

26. Ellebedy, A. et al. SARS-CoV-2 infection induces long-lived bone marrow plasma cells in humans. *Res. Square* https://doi.org/10.21203/rs.3.rs-132821/v1 (2020).

27. Hassan, A. O. et al. A single-dose intranasal chad vaccine protects upper and lower respiratory tracts against SARS-CoV-2. *Cell* 183, 169–184 (2020).

28. Bricker, T.L. et al. A single intranasal or intramuscular immunization with chimpanzee adenovirus vectored SARS-CoV-2 vaccine protects against pneumonia in hamsters. Preprint at *bioRxiv* https://doi.org/10.1101/2020.12.02.408823 (2020).

29. Hassan, A.O. et al. A single intranasal dose of chimpanzee adenovirus-vectored vaccine protects against SARS-CoV-2 infection in rhesus macaques. Preprint at *bioRxiv* https://doi.org/10.1101/2021.01.26.428251 (2021).

30. Polack, F. P. et al. Safety and efficacy of the BNT162b2 mRNA Covid-19 vaccine. *N. Engl. J. Med.* 383, 2603–2615 (2020).

31. Greaney, A. J. et al. Complete mapping of mutations to the SARS-CoV-2 spike receptor-binding domain that escape antibody recognition. *Cell Host Microbe* 29, 44–57 (2021).

32. Piccoli, L. et al. Mapping Neutralizing and immunodominant sites on the SARS-CoV-2 spike receptor-binding domain by structure-guided high-resolution serology. *Cell* 183, 1024–1042 (2020).

33. Weisblum, Y. et al. Escape from neutralizing antibodies by SARS-CoV-2 spike protein variants. *eLife* 9, e61312 (2020).

34. Liu, Z. et al. Identification of SARS-CoV-2 spike mutations that attenuate monoclonal and serum antibody neutralization. *Cell Host Microbe* https://doi.org/10.1016/j.chom.2021.01.014 (2021).

35. Andreano, E. et al. SARS-CoV-2 escape in vitro from a highly neutralizing COVID-19 convalescent plasma. Preprint at *bioRxiv* https://doi.org/10.1101/2020.12.28.424451 (2020).

36. Jangra, S. et al. The E484K mutation in the SARS-CoV-2 spike protein reduces but does not abolish neutralizing activity of human convalescent and post-vaccination sera. Preprint at *medRxiv* https://doi.org/10.1101/2021.01.26.21250543 (2021).

37. Kim, J.H., Marks, F. & Clemens, J.D. Looking beyond COVID-19 vaccine phase 3 trials. *Nat. Med.* https://doi.org/10.1038/s41591-021-01230-y (2021).

38. Schäfer, A. et al. Antibody potency, effector function, and combinations in protection and therapy for SARS-CoV-2 infection in vivo. *J. Exp. Med.* 218, e20201993 (2021).

39. Winkler, E. S. et al. Human neutralizing antibodies against SARS-CoV-2 require intact Fc effector functions and monocytes for optimal therapeutic protection. *Cell* https://doi.org/10.1016/j.cell.2021.02.026 (2021).

40. Zohar, T. et al. Compromised humoral functional evolution tracks with SARS-CoV-2 mortality. *Cell* 183, 1508–1519 (2020).

41. Dan, J.M. et al. Immunological memory to SARS-CoV-2 assessed for up to 8 months after infection. *Science* https://doi.org/10.1126/science.abf4063 (2021).

42. Lipsitch, M., Grad, Y. H., Sette, A. & Crotty, S. Cross-reactive memory T cells and herd immunity to SARS-CoV-2. *Nat. Rev. Immunol.* 20, 709–713 (2020).

43. Sette, A. & Crotty, S. Adaptive immunity to SARS-CoV-2 and COVID-19. *Cell* https://doi.org/10.1016/j.cell.2021.01.007 (2021).

44. Bailey, A. L. & Diamond, M. S. A Crisp(r) new perspective on SARS-CoV-2 biology. *Cell* 184, 15–17 (2021).

45. Liu, Y. et al. Neutralizing activity of BNT162b2-elicited serum - preliminary report. *N. Engl. J. Med.* https://doi.org/10.1056/NEJMc2102017 (2021).

46. Dong, J. et al. Genetic and structural basis for recognition of SARS-CoV-2 spike protein by a two-antibody cocktail. Preprint at *bioRxiv* https://doi.org/10.1101/2021.01.27.428529 (2021).

47. Dejnirattisai, W. et al. The antigenic anatomy of SARS-CoV-2 receptor binding domain. *Cell* https://doi.org/10.1016/j.cell.2021.02.032 (2021).

48. McCallum, M. et al. N-terminal domain antigenic mapping reveals a site of vulnerability for SARS-CoV-2. Preprint at *bioRxiv* https://doi.org/10.1101/2021.01.14.426475 (2021).

49. Goddard, T. D. et al. UCSF ChimeraX: meeting modern challenges in visualization and analysis. *Protein Sci.* 27, 14–25 (2018).

Methods

Cells. Vero E6 (CRL-1586, American Type Culture Collection), Vero-TMPRSS2 (ref. [50]) (a gift of S. Ding, Washington University) and Vero-hACE2-TMPRSS2 (a gift of A. Creanga and B. Graham, National Institutes of Health (NIH)) cells were cultured at 37 °C in Dulbecco's modified Eagle medium (DMEM) supplemented with 10% fetal bovine serum (FBS), 10 mM HEPES (pH 7.3), 1 mM sodium pyruvate, 1× nonessential amino acids and 100 U ml⁻¹ of penicillin–streptomycin. Vero-TMPRSS2 cell cultures were supplemented with 5 µg ml⁻¹ of blasticidin. TMPRSS2 expression was confirmed using an anti-V5 antibody (Thermo Fisher Scientific, 2F11F7) or anti-TMPRSS2 mAb (Abnova, Clone 2F4) and APC-conjugated goat anti-mouse IgG (BioLegend, 405308). Vero-hACE2-TMPRSS2 cell cultures were supplemented with 10 µg ml⁻¹ of puromycin.

Viruses. The 2019n-CoV/USA_WA1/2020 isolate of SARS-CoV-2 was obtained from the US Centers for Disease Control. The B.1.1.7 isolate was obtained from an infected individual. Individual point mutations in the spike gene (D614G, K417N/D614G, E484K/D614G, N501Y/D614G, P681H/D614G, del69-70/N501Y/D614G and E484K/N501Y/D614G) were introduced into an infectious complementary DNA clone of the 2019n-CoV/USA_WA1/2020 (WA1/2020) strain as described previously[51]. Nucleotide substitutions were introduced into a subclone puc57-CoV-2-F5-7 containing the spike gene of the SARS-CoV-2 wild-type infectious clone[52]. The South African (B.1.351) and Brazilian (B.1.1.248) variant spike genes were produced synthetically by Gibson assembly. The full-length infectious cDNA clones of the variant SARS-CoV-2 viruses were assembled by in vitro ligation of seven contiguous cDNA fragments following the previously described protocol[52]. In vitro transcription was then performed to synthesize full-length genomic RNA. To recover the mutant viruses, RNA transcripts were electroporated into Vero E6 cells. Viruses from the supernatant of cells were collected 40 h later and served as p0 stocks[53]. All viruses were passaged once in Vero-hACE2-TMPRSS2 or Vero-TMPRSS2 cells and subjected to deep sequencing after RNA extraction to confirm the introduction and stability of substitutions (Supplementary Table 1). Viral RNA from cell culture supernatants was used to generate next-generation sequencing libraries using either the Illumina TruSeq Stranded Total RNA Library Prep with Ribo-Zero kit or the Illumina Stranded Total RNA Prep, Ligation with Ribo-Zero Plus kit per the manufacturer's protocol. The final indexed libraries were quantified using Agilent's Bioanalyzer and pooled at an equal molar concentration. Illumina's NextSeq sequencer was used to generate paired-end 150-base-pair reads. Raw sequencing data were processed using fastp[54] v.0.20.1 (https://github.com/OpenGene/fastp) to trim adaptors and filter out sequences with <Q30. Alignment to the SARS-CoV-2 reference genome (MN908947.3) was performed using BWA[55] v.0.7.17-r1188 (http://bio-bwa.sourceforge.net). DeepVariant[56] v.1.1.0 (https://github.com/google/deepvariant) was used to call variants with an allele frequency ≥50%. Variants were annotated using SNPEff[57] 5.0c (https://sourceforge.net/projects/snpeff/). All virus preparation and experiments were performed in an approved Biosafety level 3 facility.

Monoclonal antibodies. The human mAbs studied in this paper (COV2-2196, COV2-2072, COV2-2050, COV2-2381, COV2-2130, COVOX-384, COVOX-40, S309, S2E12, S2H58, S2X333, VIR-7381 and S2X259) were isolated from blood samples from individuals in North America or Europe with previous laboratory-confirmed symptomatic SARS-CoV or SARS-CoV-2 infection. The original clinical studies to obtain specimens after written informed consent were previously described[3,5,7,47,48] and approved by the Institutional Review Board of Vanderbilt University Medical Center, the Institutional Review Board of the University of Washington, the Research Ethics Board of the University of Toronto and the Canton Ticino Ethics Committee (Switzerland). Chimeric mAb 1B07 with a murine Fv and human Fc (human IgG1) were isolated from C57BL/6 mice immunized with recombinant spike and RBD proteins and described previously[20]. Murine mAbs were generated in BALB/c or C57BL/6 mice immunized with recombinant spike and RBD proteins and described previously[34].

Human immune sera. Multiple sources of human serum samples were used in this study: Convalescent serum samples were obtained from a cohort recruited from the St. Louis metropolitan area who experienced mild SARS-CoV-2 infection. None of those patients required intubation and the study was approved by Washington University School of Medicine Institutional Review Board (202003186 (WU353)). The serum samples from individuals immunized with the Pfizer-BioNTech (BNT162b2) mRNA vaccine were obtained before primary immunization or 1 week after boosting from young adults and the studies were approved by Washington University School of Medicine Institutional Review Board (202012081 (WU368) and 202012084 (COVaRiPAD)).

Mouse, hamster and NHP immune sera. The mouse, hamster and NHP immune sera were obtained 1 month after intranasal immunization with ChAd-SARS-CoV-2, a chimpanzee adenoviral vectored vaccine encoding for a prefusion stabilized form of the spike protein. Details of the immunization protocol and functional analyses have been described elsewhere[27–29].

Focus reduction neutralization test. Serial dilutions of mAbs (starting at 10 µg ml⁻¹ dilution) or serum were incubated with 10² focus-forming units of different strains or variants of SARS-CoV-2 for 1 h at 37 °C. Antibody–virus complexes were added to Vero-hACE2-TMPRSS2 or Vero-TMPRSS2 cell monolayers in 96-well plates and incubated at 37 °C for 1 h. Subsequently, cells were overlaid with 1% (w/v) methylcellulose in MEM supplemented with 2% FBS. Plates were collected 24 h later by removing overlays and fixed with 4% PFA in PBS for 20 min at room temperature. Plates were washed and sequentially incubated with an oligoclonal pool of SARS2-2, SARS2-11, SARS2-16, SARS2-31, SARS2-38, SARS2-57 and SARS2-71 anti-S antibodies and HRP-conjugated goat anti-mouse IgG (Sigma, 12-349) in PBS supplemented with 0.1% saponin and 0.1% bovine serum albumin. SARS-CoV-2-infected cell foci were visualized using TrueBlue peroxidase substrate (KPL) and quantitated on an ImmunoSpot microanalyzer (Cellular Technologies).

ELISA. Assays were performed in 96-well plates (MaxiSorp; Thermo) coated with 100 µl of recombinant spike or RBD protein[20] in PBS and plates were incubated at 4 °C overnight. Plates were then blocked with 10% FBS and 0.05% Tween-20 in PBS. Serum were serially diluted in blocking buffer and added to the plates. Plates were incubated for 90 min at room temperature and then washed three times with 0.05% Tween-20 in PBS. Goat anti-human IgG-HRP (Jackson ImmunoResearch, 115-035-003; 1:2,500 dilution) was incubated in blocking buffer before adding to wells and incubating for 60 min at room temperature. Plates were washed three times with 0.05% Tween-20 in PBS and then washed three times with PBS before the addition of peroxidase substrate (SigmaFAST o-phenylenediamine dihydrochloride, Sigma-Aldrich). Reactions were stopped by the addition of 1 M HCl. Optical density measurements were taken at 490 nm. The half-maximal binding dilution for each serum or plasma sample was calculated using nonlinear regression. The limit of detection was defined as 1:30.

Transient expression of recombinant SARS-CoV-2 spike proteins and flow cytometry. The full-length S gene of SARS-CoV-2 strain (SARS-CoV-2-S) isolate BetaCoV/Wuhan-Hu-1/2019 (accession number MN908947) carrying D614G was codon-optimized for expression in hamster cells and cloned into the pcDNA3 expression vector. Amino acid substitutions for B.1.1.7, P.1 (Brazilian lineage: L18F, T20N, P26S, D138Y, R190S, K417T, E484K, N501Y, H655Y, T1027I and V1167F) and B.1.351 variants were introduced by overlap extension PCR. Briefly, DNA fragments with overlap sequences were amplified by PCR (step 1). Mutations were introduced by amplification with primers with similar melting points. Deletion of the C-terminal 21 amino acids was introduced to increase surface expression of the recombinant spike. Next, three contiguous overlapping fragments were fused by a first overlap PCR (step 2) using the utmost external primers of each set, resulting in three larger fragments with overlapping sequences. A final overlap PCR (step 3) was performed on the three large fragments using the utmost external primers to amplify the S gene and the flanking sequences including the restriction sites KpnI and NotI. This fragment was digested and cloned into the expression plasmid phCMV1. For all PCR reactions, Q5 Hot Start High fidelity DNA polymerase was used (New England Biolabs) according to manufacturer's instructions and adapting the elongation time to the size of the amplicon. After each PCR step, the amplified regions were separated on agarose gel and purified using Illustra GFX PCR DNA and a Gel Band Purification kit (Merck KGaA).

ExpiCHO cells (Thermo Fisher Scientific, A29127) were transiently transfected with SARS-CoV-2-S expression vectors using Expifectamine CHO Enhancer. Two days later, cells were collected for immunostaining with mAbs. Binding of mAbs to transfected cells was analyzed by flow cytometry using a ZE5 Cell Analyzer (Biorard) and FlowJo software (v.9, TreeStar). Positive binding was defined by differential staining of CoV-S transfectants versus mock transfectants.

SARS-CoV-2 pseudotyped virus production. The 293T/17 cells (American Type Culture Collection CRL-11268) were seeded in 10-cm dishes for 80% next day confluency. The next day, cells were transfected with the plasmid pcDNA3.1(+)-spike-D19 (encoding the SARS-CoV-2 spike protein) or pcDNA3.1(+)-spike-D19 variants using the transfection reagent TransIT-Lenti according to the manufacturer's instructions. One day after transfection, cells were infected with VSV-luc(VSV-G) at a multiplicity of infection of 3. The cell supernatant containing SARS-CoV-2 pseudotyped virus was collected at day 2 after transfection, centrifuged at 1,000g for 5 min to remove cellular debris, aliquoted and frozen at −80 °C. The SARS-CoV-2 pseudotyped virus preparation was quantified using Vero E6 cells seeded at 20,000 cells per well in clear bottom black 96-well plates the previous day. Cells were inoculated with 1:10 dilution series of pseudotyped virus in 50 µl DMEM for 1 h at 37 °C. An additional 50 µl of DMEM was added, cells were incubated overnight at 37 °C. Luciferase activity was quantified with Bio-Glo reagent by adding 100 µl of Bio-Glo (diluted 1:1 in PBS), incubated at room temperature for 5 min and relative light units were read on an EnSight or EnVision plate reader.

Neutralization of SARS-CoV-2 pseudotyped virus. Vero E6 cells were seeded into clear bottom black-walled 96-well plates at 20,000 cells per well in 100 µl medium and cultured overnight at 37 °C. Twenty-four hours later, 1:3 8-point serial dilutions of mAb were prepared in medium, with each dilution tested in duplicate on each plate (range: 10 µg ml⁻¹ to 4 ng ml⁻¹ final concentration).

Pseudovirus was diluted 1:25 in medium and added 1:1 to 110 μl of each antibody dilution. Pseudovirus:antibody mixtures were incubated for 1 h at 37 °C. Medium was removed from the Vero E6 cells and 50 μl of pseudovirus:antibody mixtures were added to the cells. One hour after infection, 100 μl of medium was added to wells containing pseudovirus:antibody mixtures and incubated for 17 h at 37 °C. Medium then was removed and 100 μl of Bio-Glo reagent (diluted 1:1 in DPBS) was added to each well. The plate was shaken on a plate shaker at 300 r.p.m. at room temperature for 20 min and relative light units were read on an EnSight or EnVision plate reader.

Statistical analysis. All statistical tests were performed as described in the indicated figure legends. Nonlinear regression curve fitting was performed to calculate EC_{50} values. Statistical significance was calculated using a nonparametric two-tailed Wilcoxon matched-pairs signed-rank test and Prism 8.0. The number of independent experiments used are indicated in the relevant figure legends.

Reporting Summary. Further information on research design is available in the Nature Research Reporting Summary linked to this article.

Data availability
All data supporting the findings of this study are available within the paper and are available from the corresponding author upon request. Deep sequencing datasets of viral stocks are available at NCBI BioProject PRJNA698378. Source data are provided with this paper.

References
50. Zang, R. et al. TMPRSS2 and TMPRSS4 promote SARS-CoV-2 infection of human small intestinal enterocytes. *Sci. Immunol.* **5**, eabc3582 (2020).
51. Plante, J.A. et al. Spike mutation D614G alters SARS-CoV-2 fitness. *Nature* https://doi.org/10.1038/s41586-020-2895-3 (2020).
52. Xie, X. et al. An infectious cDNA clone of SARS-CoV-2. *Cell Host Microbe* **27**, 841–848 (2020).
53. Xie, X. et al. Engineering SARS-CoV-2 using a reverse genetic system. *Nat. Protoc.* https://doi.org/10.1038/s41596-021-00491-8 (2021).
54. Chen, S., Zhou, Y., Chen, Y. & Gu, J. fastp: an ultra-fast all-in-one FASTQ preprocessor. *Bioinformatics* **34**, i884–i890 (2018).
55. Li, H. & Durbin, R. Fast and accurate short read alignment with Burrows–Wheeler transform. *Bioinformatics* **25**, 1754–1760 (2009).
56. Poplin, R. et al. A universal SNP and small-indel variant caller using deep neural networks. *Nat. Biotechnol.* **36**, 983–987 (2018).
57. Cingolani, P. et al. A program for annotating and predicting the effects of single nucleotide polymorphisms, SnpEff: SNPs in the genome of *Drosophila melanogaster* strain w1118; iso-2; iso-3. *Fly* **6**, 80–92 (2012).

Author contributions
R.E.C. and J.B.C. performed and analyzed neutralization assays. D.P. carried out pseudovirus neutralization and flow cytometry assays. X.X., Y.L., J.L. and X.Z. designed and generated isogenic SARS-CoV-2 variant viruses. S.T., L.D. and D.W. performed deep sequencing analysis. A.H.E., R.M.P., J.A.O., A.H.J.K. and P.D. designed and supervised clinical studies and J.S.T., W.K., M.T. and A.J.S. obtained and characterized clinical samples. A.C.M.B. provided hamster immune sera. D.C., N.S., P.G., S.J.Z., J.E.C., A.E. and H.W.V. provided mAbs and performed analyses. P.-Y.S., A.H.E., D.C. and M.S.D. obtained funding and supervised the research. R.E.C, J.B.C., E.S.W., H.W.V. and M.S.D. wrote the initial draft, with the other authors providing editorial comments.

Additional information
Extended data is available for this paper at https://doi.org/10.1038/s41591-021-01294-w.

Supplementary information The online version contains supplementary material available at https://doi.org/10.1038/s41591-021-01294-w.

Correspondence and requests for materials should be addressed to A.H.E., P.-Y.S. or M.S.D.

Peer review information *Nature Medicine* thanks Stanley Perlman and the other, anonymous reviewer(s) for their contribution to the peer review of this work. Joao Monteiro was the primary editor on this article and managed its editorial process and peer review in collaboration with the rest of the editorial team.

Reprints and permissions information is available at www.nature.com/reprints.
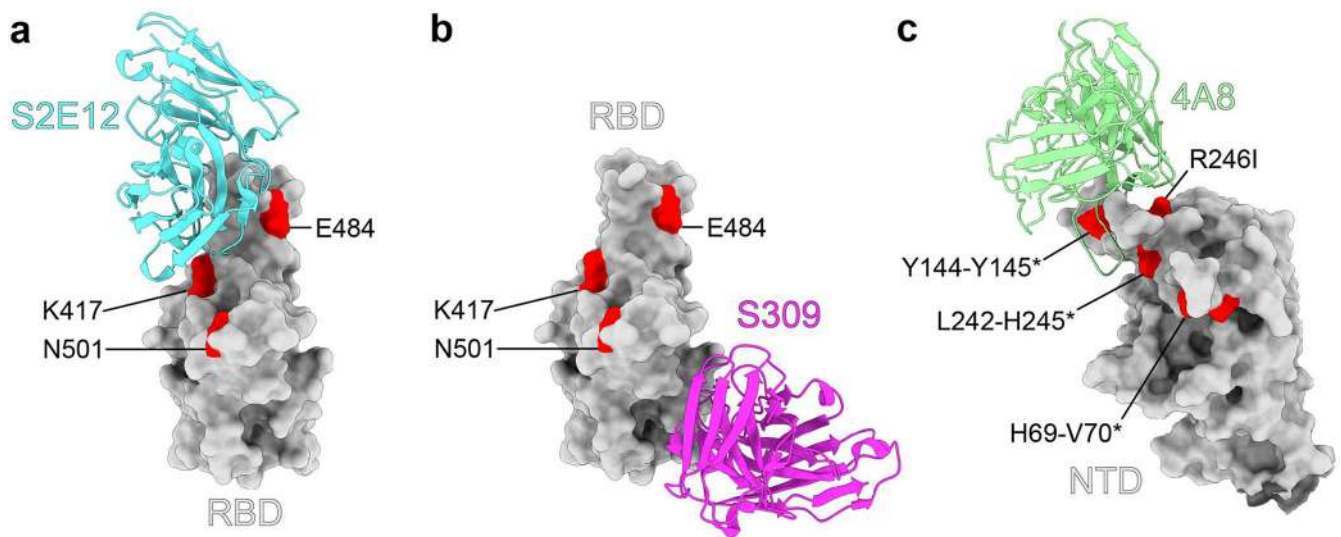
Extended Data Fig. 1 | MAb-spike structures. Structures of the SARS-CoV-2 RBD in complex with a representative neutralizing antibody from (**a**) class 1 (S2E12, PDB: 7K45), or (**b**) class 2 (S309, PDB: 6WPS). **c**, Structure of the SARS-CoV-2 spike N-terminal domain (NTD) in complex with a representative class 3 neutralizing antibody (4A8, PDB: 7C2L). All structural analysis and figures were generated with UCSF ChimeraX[49].
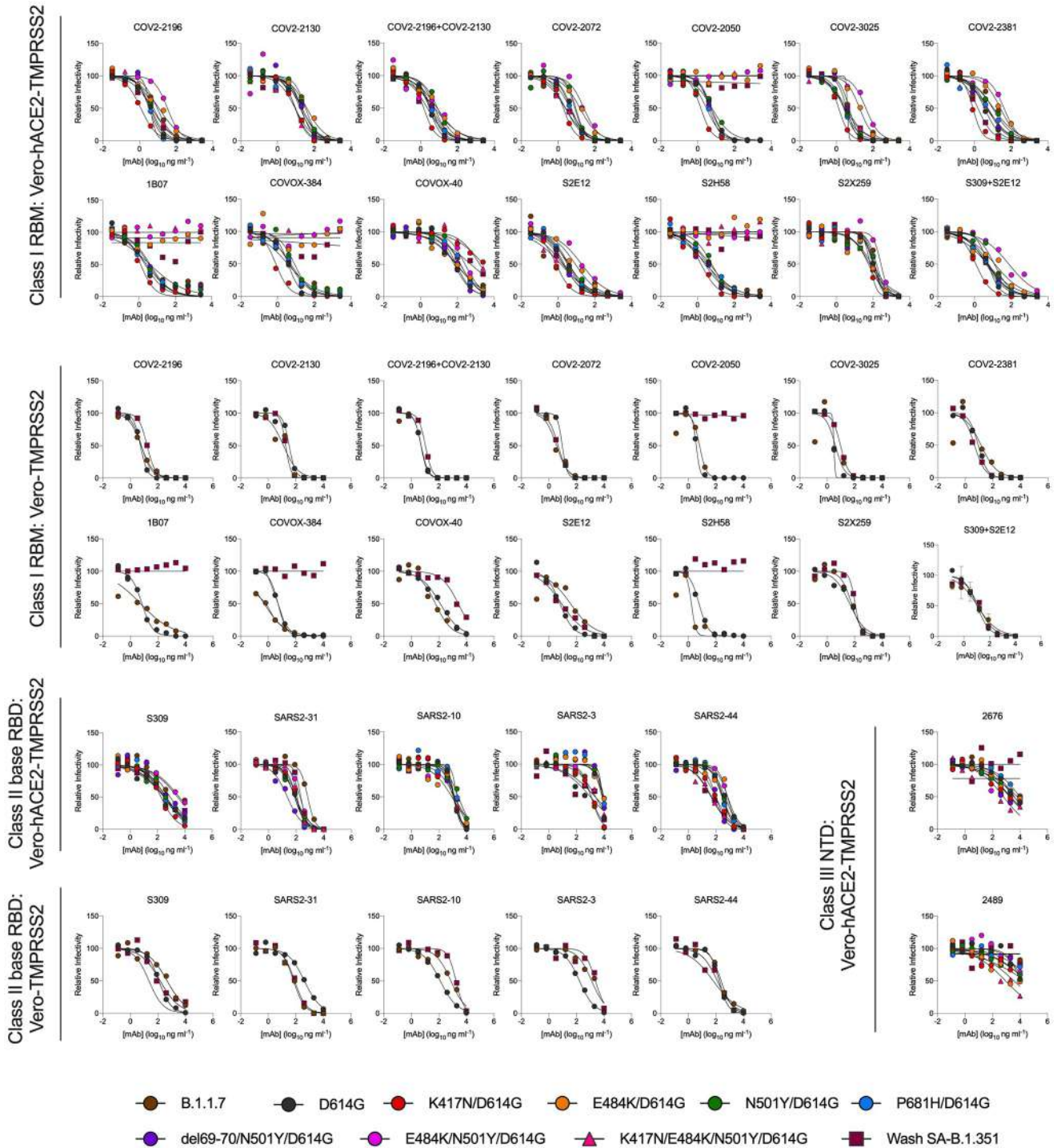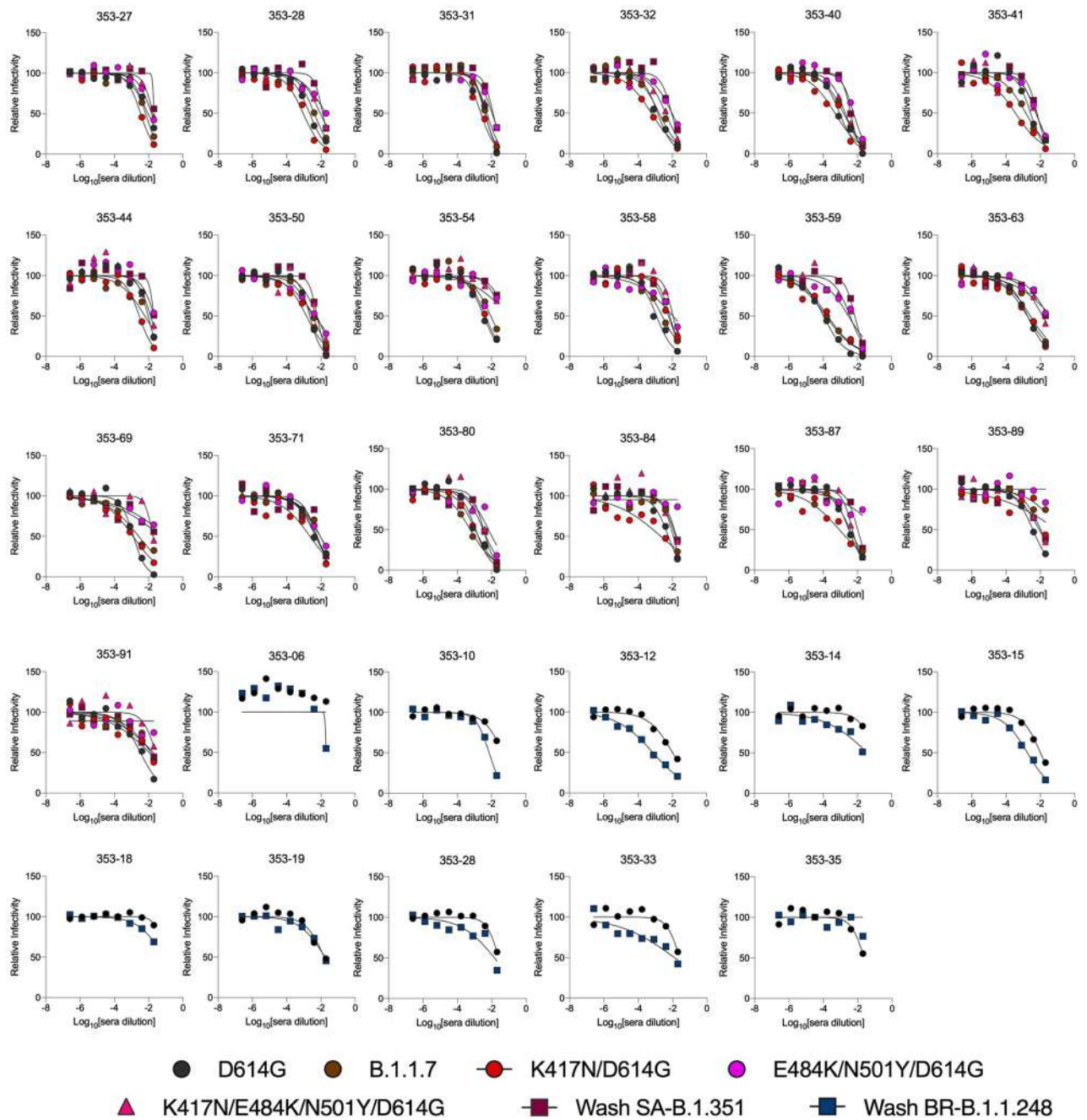
Extended Data Fig. 2 | Neutralization curves with mAbs and variant SARS-CoV-2 strains. Anti-SARS-CoV-2 human mAbs were tested for neutralization of infection of the indicated viral variants and isolates using a FRNT on Vero-hACE2-TMPRSS2 or Vero-TMPRSS2 cells. One representative experiment of two performed in duplicate is shown.
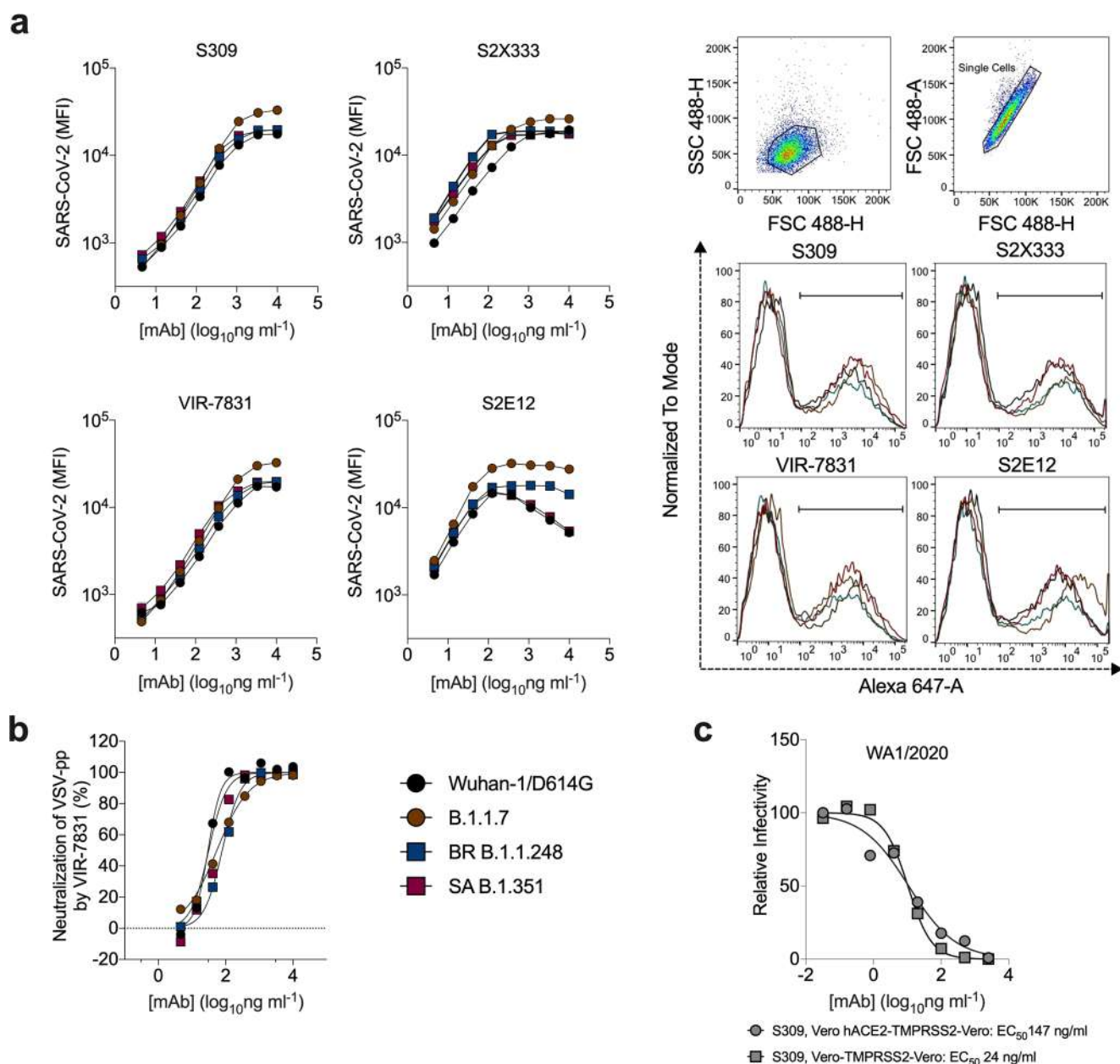
Extended Data Fig. 3 | Binding and neutralizing activity of mAbs to SARS-CoV-2 variants. a, Binding of mAbs S2E12 (class 1, RBM), S309 (class 2, RBD base), VIR-7381 (class 2, RBD base) and S2X333 (class 3, NTD) to SARS-CoV-2 spike proteins from the indicated strains when expressed on the surface of ExpiCHO cells (symbols, mean of duplicates from one experiment). Gating strategy and binding of mAbs S2E12, S309, VIR-7831, and S2X333 (at 370 ng/mL) to SARS-CoV-2 spike from indicated variants when expressed on the surface of ExpiCHO cells. Shown on histograms is the gating strategy of the population of positive cells (percentage ranging between 37 and 46%) used to calculate MFI. **b**, Neutralization of VSV-SARS-CoV-2 pseudotyped viruses (with indicated spike proteins) on Vero E6 cells. Mean ± standard deviation of sextuplicates is shown for all pseudoviruses, except for SARS-CoV-2 WT (mean of triplicates). WT, Wuhan-1 + D614G. **c**, Serial dilutions of S309 mAb were mixed with Vero CCL81 cell-derived WA1/2020 and added to Vero-hACE2-TMPRSS2 or Vero-TMPRSS2 cells for evaluation of neutralizing activity by FRNT. One representative experiment of two is shown. The EC50 values are provided in the legend in ng/mL.
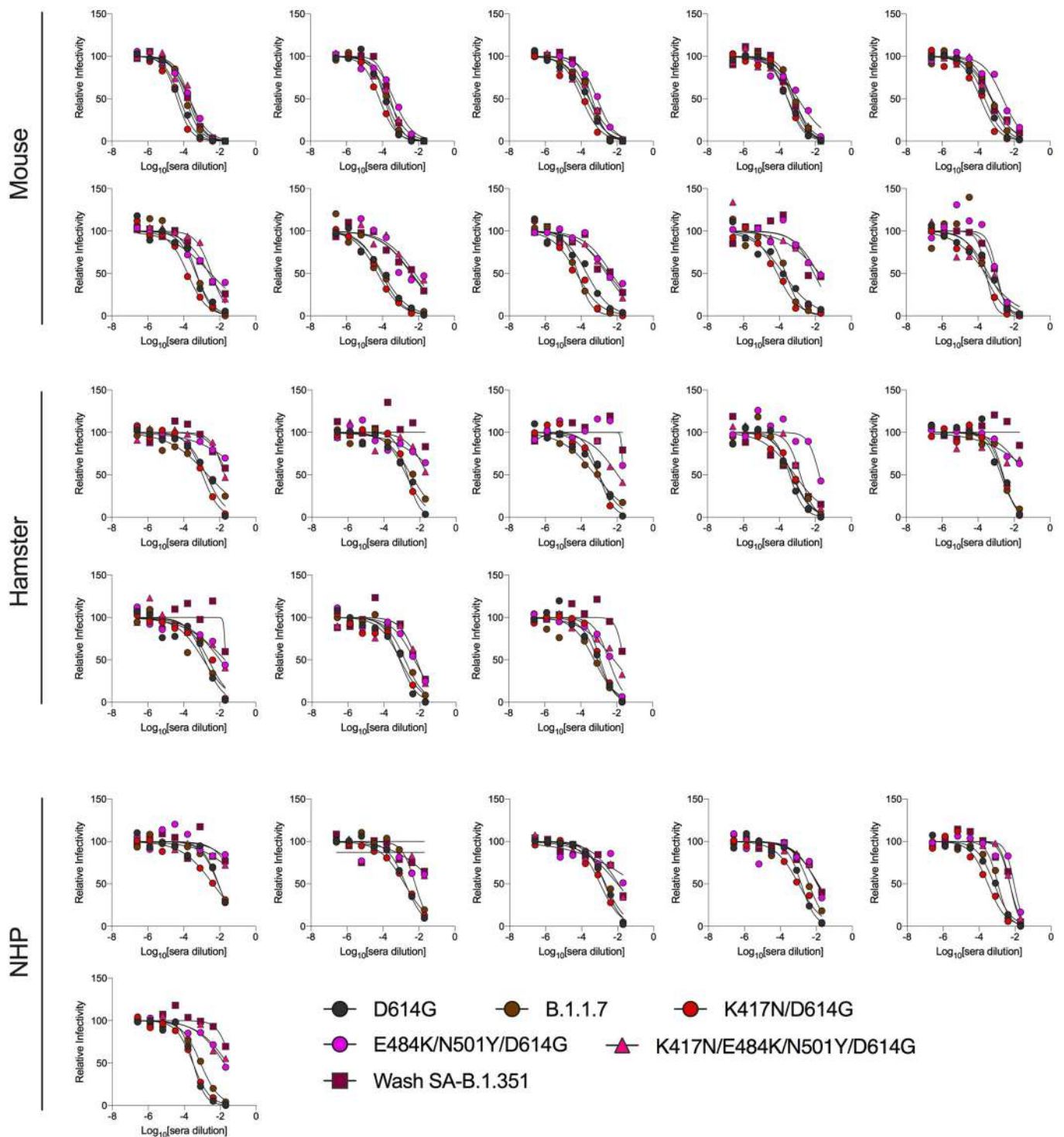
Extended Data Fig. 4 | Neutralization curves with convalescent human sera from longitudinal cohort and variant SARS-CoV-2 strains. Serum from individuals (n = 29) who had been infected with SARS-CoV-2 (samples obtained at ~1-month post-infection) were tested for neutralization of the indicated viral variants and isolates in Vero-hACE2-TMPRSS2 cells using a FRNT. One experiment performed in duplicate is shown.
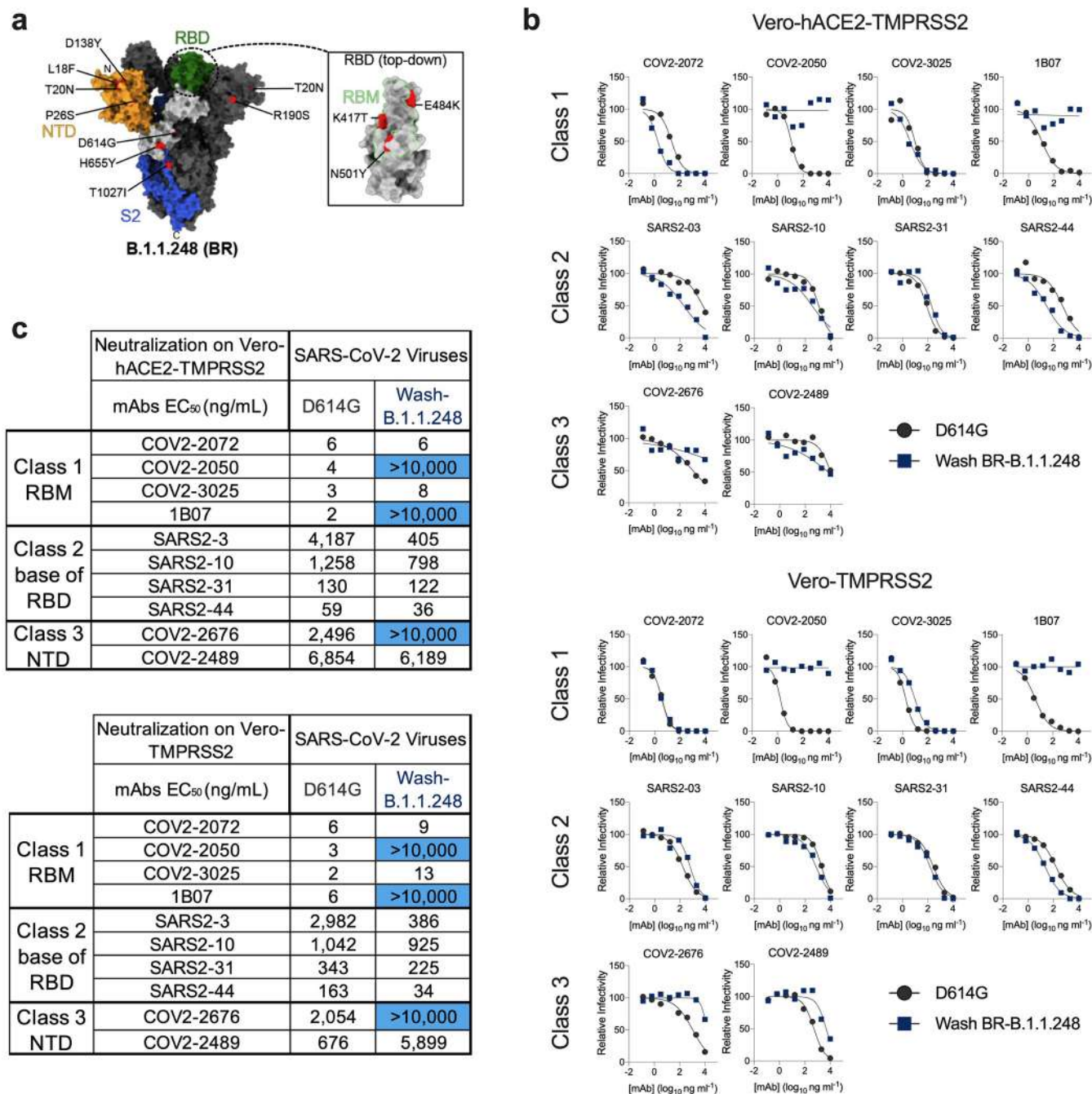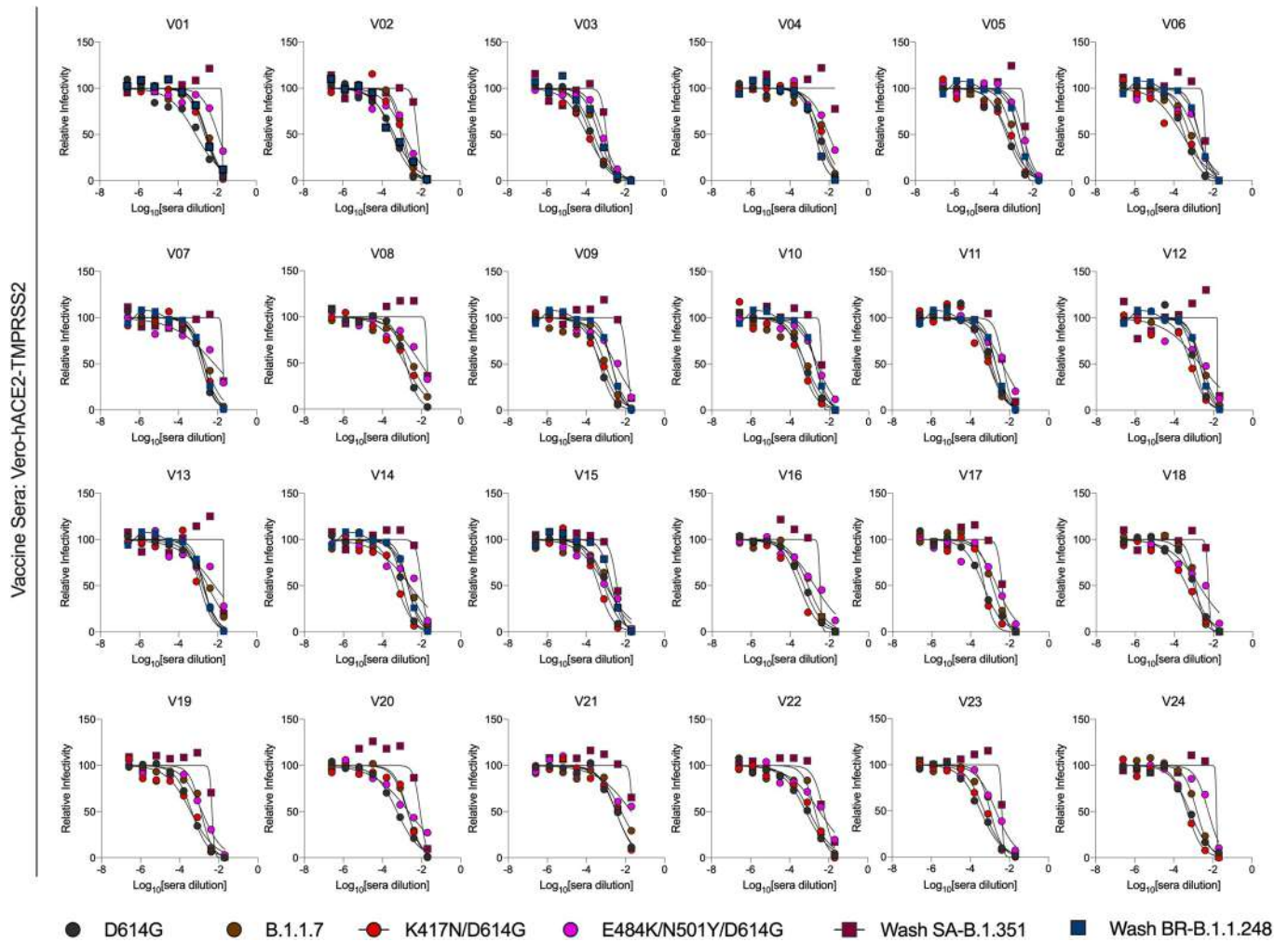
Extended Data Fig. 5 | Neutralization curves with mAbs and Wash BR-B.1.1.248 virus. a, Surface representation of SARS-CoV-2 spike showing the NTD in orange, RBD in green, and S2 portion of the molecule in blue, with N- and C-termini annotated. Substitutions seen in the B.1.1.248 Brazilian variant (L18F, T20N, P26S, D138Y, R190S, K417T, E484K, N501Y, D614G, H655Y, T1027I, and V1176F) are shaded red. Red hexagon depicts approximate location of R190S, which is obscured in this view. Red star indicates approximate location of T1027I, which is obscured in this view. V1176F is not shown, as it exists beyond the C-terminus of this model, which ends at residue D1146. Inset shows top-down view of the RBD with B.1.1.248 RBD substitutions (K417T/E484K/N501Y) shaded red and contextualized with the receptor-binding motif. Spike was modelled using PDB: 7C2L; RBD was modelled using PDB: 6W41. All structural analyses and figures were generated with UCSF ChimeraX[49]. **b,** Selected anti-SARS-CoV-2 human mAbs (selected ones used are indicated) were tested for neutralization of the indicated Wash BR-B.1.1.248 using a FRNT on Vero-hACE2-TMPRSS2 cells (*top*) or on Vero -TMPRSS2 cells (*bottom*). One representative experiment of two performed in duplicate is shown. **c,** Summary of EC_{50} values (ng/ml) of neutralization of Wash BR-B.1.1.248 performed in Vero-hACE2-TMPRSS2 cells (*top*) or on Vero-TMPRSS2 cells (*bottom*). Data are an average of two experiments, each performed in duplicate. Blue shading of cells shows virtually complete loss of neutralizing activity: $EC_{50} > 10,000$ ng/mL.
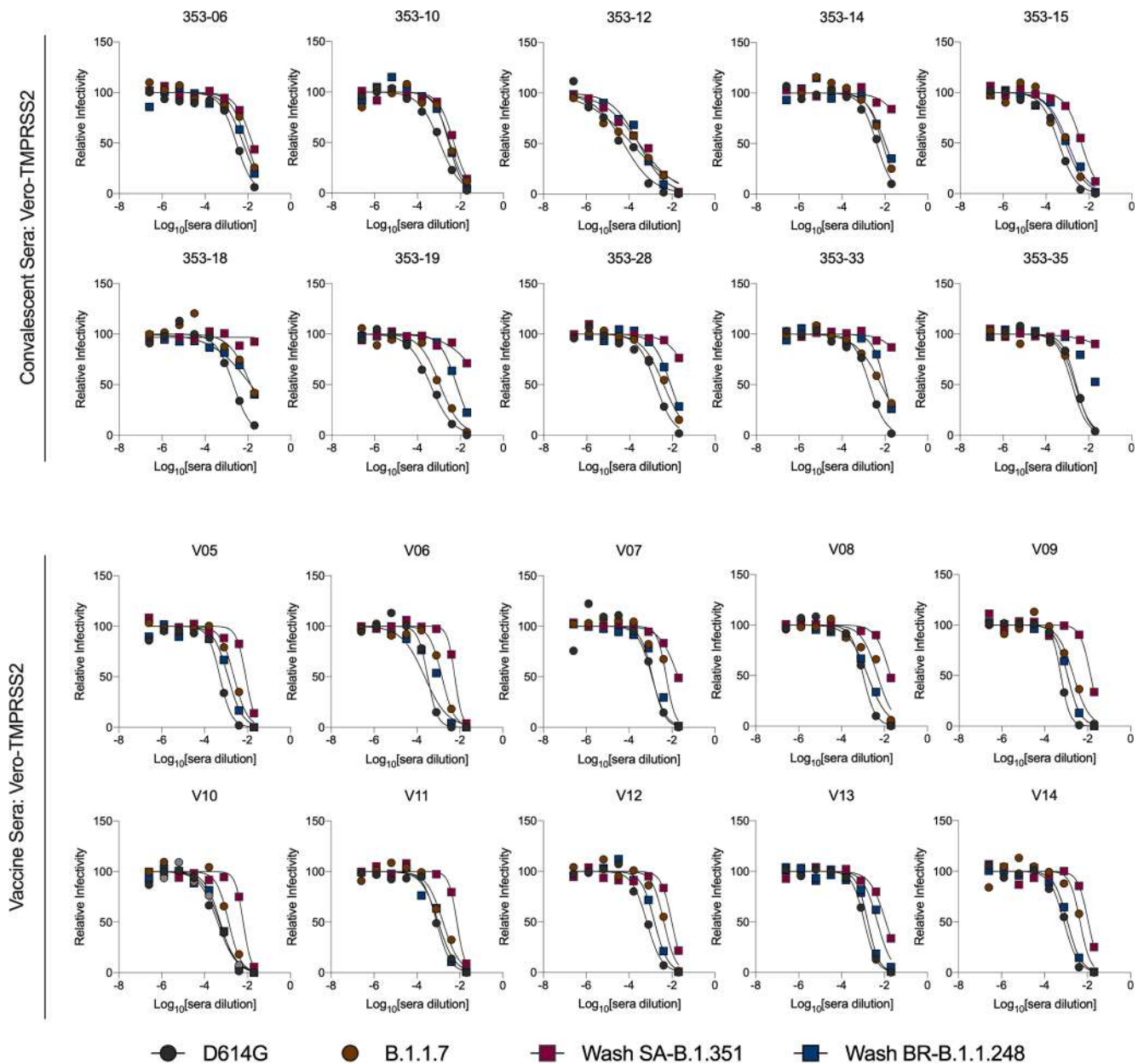
Extended Data Fig. 6 | Neutralization curves with animal sera from ChAd-CoV-2 vaccinated animals and variant SARS-CoV-2 strains. Serum samples were collected from mice (n=10), hamsters (n=8), or rhesus macaques (NHP, n=6) ~30 days after a single intranasal immunization with ChAd-SARS-CoV-2-S. Sera were tested for neutralization of infection of the indicated viral variants and isolates in Vero-hACE2-TMPRSS2 cells using a FRNT. One experiment performed in duplicate is shown.
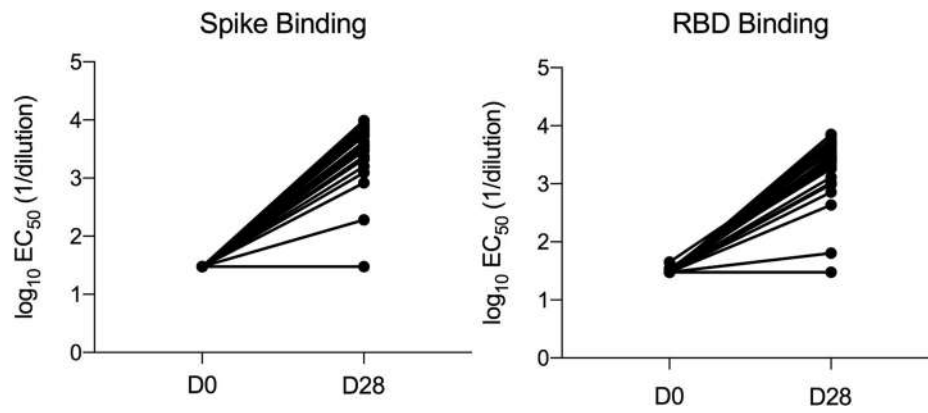
Extended Data Fig. 7 | S and RBD binding activity of human sera from individuals vaccinated with BNT162b2 mRNA vaccine. Individuals were vaccinated and boosted with the Pfizer-BioNTech mRNA vaccine. At seven days after boosting, sera were collected and tested for binding to S or RBD proteins (WA1/2020 strain) by ELISA. One experiment performed in duplicate is shown.

Extended Data Fig. 8 | Neutralization curves in Vero-hACE2-TMPRSS2 cells with human sera from subjects vaccinated with the BNT162b2 mRNA vaccine and variant SARS-CoV-2 strains. Individuals were vaccinated and boosted with the Pfizer-BioNTech mRNA vaccine. Sera were collected and tested for neutralization of infection of the indicated viral variants and isolates using a FRNT and Vero-hACE2-TMPRSS2 cells. One experiment performed in duplicate is shown.

Extended Data Fig. 9 | Neutralization curves of variant SARS-CoV-2 strains in Vero-TMPRSS2 cells with human sera from convalescent subjects or those vaccinated with the BNT162b2 mRNA vaccine. Serum from individuals (n = 10) who had been infected with SARS-CoV-2 (~ 1-month time point) or vaccinated with the Pfizer-BioNTech mRNA vaccine (n = 10) were tested for neutralization of the indicated SARS-CoV-2 strains (D614G, B.1.1.7, Wash SA-B.1.351, Wash BR-B.1.248) using a FRNT and Vero-TMPRSS2 cells. One experiment performed in duplicate is shown, with some exceptions due to limited sample.
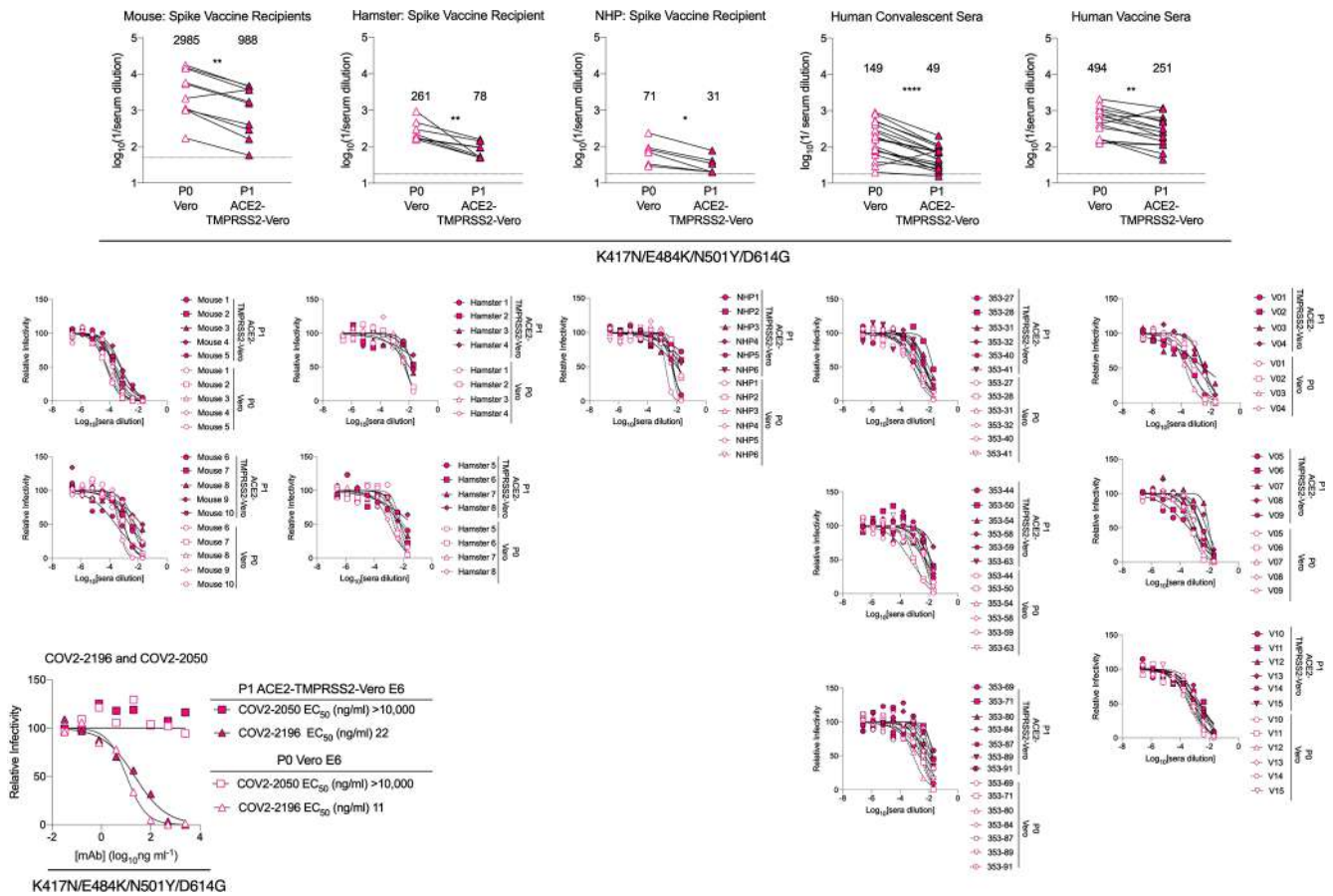
Extended Data Fig. 10 | Differential serum neutralization of SARS-CoV-2 produced in Vero E6 and Vero-hACE2-TMPRSS2 cells. ((*Top panels*) Immune or vaccine-derived sera from mice, hamsters, NHP, or humans (see Figs. 2–4) were incubated with deep-sequenced confirmed p0 (Vero cell-produced) or p1 (Vero-hACE2-TMPRSS2 cell-produced) versions of K417N/E484K/N501Y/D614G virus and then subjected to a FRNT in Vero-hACE2-TMPRSS2 recipient cells. EC_{50} values were calculated from one experiment performed in duplicate. GMT values are shown above each graph. Dotted line represents the limit of detection of the assay. Two-tailed Wilcoxon matched-pairs signed rank test: Mouse vaccine sera, $P = 0.0039$; Hamster vaccine sera, $P = 0.0078$; NHP vaccine sera, $P = 0.0312$; Human convalescent sera, $P = 0.0001$; Human vaccine sera, $P = 0.0026$. (*Middle panels*) Serum neutralization curves with K417N/E484K/N501Y/D614G virus (p0, generated in Vero E6 cells; p1, generated in Vero-hACE2-TMPRSS2 cells) using a FRNT and Vero-hACE2-TMPRSS2 cells. One experiment performed in duplicate is shown. (*Bottom left panel*) Neutralization curves and EC_{50} values with COV2-2050 and COV2-2196 mAbs using the p0 (Vero cell-produced) or p1 (Vero-hACE2-TMPRSS2 cell-produced) viruses and recipient Vero-hACE2-TMPRSS2 cells.

Corresponding author(s):   Michael Diamomd

Last updated by author(s):   Feb 19, 2021

Reporting Summary

Nature Research wishes to improve the reproducibility of the work that we publish. This form provides structure for consistency and transparency in reporting. For further information on Nature Research policies, see our Editorial Policies and the Editorial Policy Checklist.

Statistics

For all statistical analyses, confirm that the following items are present in the figure legend, table legend, main text, or Methods section.

n/a	Confirmed	
☐	☒	The exact sample size (*n*) for each experimental group/condition, given as a discrete number and unit of measurement
☐	☒	A statement on whether measurements were taken from distinct samples or whether the same sample was measured repeatedly
☐	☒	The statistical test(s) used AND whether they are one- or two-sided
		Only common tests should be described solely by name; describe more complex techniques in the Methods section.
☒	☐	A description of all covariates tested
☒	☐	A description of any assumptions or corrections, such as tests of normality and adjustment for multiple comparisons
☐	☒	A full description of the statistical parameters including central tendency (e.g. means) or other basic estimates (e.g. regression coefficient) AND variation (e.g. standard deviation) or associated estimates of uncertainty (e.g. confidence intervals)
☐	☒	For null hypothesis testing, the test statistic (e.g. *F*, *t*, *r*) with confidence intervals, effect sizes, degrees of freedom and *P* value noted
		Give P values as exact values whenever suitable.
☒	☐	For Bayesian analysis, information on the choice of priors and Markov chain Monte Carlo settings
☒	☐	For hierarchical and complex designs, identification of the appropriate level for tests and full reporting of outcomes
☒	☐	Estimates of effect sizes (e.g. Cohen's *d*, Pearson's *r*), indicating how they were calculated

Our web collection on statistics for biologists contains articles on many of the points above.

Software and code

Policy information about availability of computer code

Data collection	No software was used in this study to collect data
Data analysis	Prism 8.0 was used to perform all statistical analysis. BWA4 v0.7.17-r1188 (http://bio-bwa.sourceforge.net). DeepVariant4 v1.1.0 (https://github.com/google/deepvariant) was used to call variants with an allele frequency >= 50%. Variants were annotated using SNPEff4 5.0c (https://sourceforge.net/projects/snpeff/). FlowJo software (v9) was used for analysis of flow cytometry

For manuscripts utilizing custom algorithms or software that are central to the research but not yet described in published literature, software must be made available to editors and reviewers. We strongly encourage code deposition in a community repository (e.g. GitHub). See the Nature Research guidelines for submitting code & software for further information.

Data

Policy information about availability of data

All manuscripts must include a data availability statement. This statement should provide the following information, where applicable:
- Accession codes, unique identifiers, or web links for publicly available datasets
- A list of figures that have associated raw data
- A description of any restrictions on data availability

All data supporting the findings of this study are available within the paper and are available from the corresponding author upon request. Deep sequencing datasets of viral stocks are available at NCBI BioProject PRJNA698378 (https://www.ncbi.nlm.nih.gov/bioproject/PRJNA698378).

Field-specific reporting

Please select the one below that is the best fit for your research. If you are not sure, read the appropriate sections before making your selection.

☒ Life sciences ☐ Behavioural & social sciences ☐ Ecological, evolutionary & environmental sciences

For a reference copy of the document with all sections, see nature.com/documents/nr-reporting-summary-flat.pdf

Life sciences study design

All studies must disclose on these points even when the disclosure is negative.

Sample size	No sample sizes were chosen a priori, as samples were used based on availability. Notwithstanding this point, each serum analysis has n =10 to 24 samples, which allows us to reliably detect 2-fold differences in potency.
Data exclusions	No data was excluded.
Replication	All experiments with monoclonal antibodies were performed at least two independent times each with two technical replicate per experiment. Serum studies were performed as one independent experiment with two technical replicates.
Randomization	No randomization was performed as we obtained available samples that were deidentified
Blinding	Blinding was not performed for convenience. However, data was scanned and analyzed by a separate investigator who did not perform the experiment.

Reporting for specific materials, systems and methods

We require information from authors about some types of materials, experimental systems and methods used in many studies. Here, indicate whether each material, system or method listed is relevant to your study. If you are not sure if a list item applies to your research, read the appropriate section before selecting a response.

Materials & experimental systems

n/a	Involved in the study
☐	☒ Antibodies
☐	☒ Eukaryotic cell lines
☒	☐ Palaeontology and archaeology
☐	☒ Animals and other organisms
☐	☒ Human research participants
☒	☐ Clinical data
☒	☐ Dual use research of concern

Methods

n/a	Involved in the study
☒	☐ ChIP-seq
☐	☒ Flow cytometry
☒	☐ MRI-based neuroimaging

Antibodies

Antibodies used	Human mAbs (all generated by the Crowe, Ellebedy, Corti and Screaton laboratiries as part of this study): COV2-2196, COV2-2072, COV2-2050, COV2-2381, COV2-2130, COVOX-384, COVOX-40, 1B07, S309, S2E12, S2H58, and S2X259; Mouse mAbs (all generated by the Diamond laboratory): SARS2-2, SARS2-11, SARS2-16, SARS2-31, SARS2-38, SARS2-57, and SARS2-71; HRP-conjugated goat anti-mouse IgG (Sigma 12-349), anti-V5 antibody (Thermo Fisher 2F11F7), anti-TMPRSS2 mAb (Abnova, Clone 2F4), APC-conjugated goat anti-mouse IgG (BioLegend, 405308), Goat anti-human IgG-HRP (Jackson ImmunoResearch, 115-035-003)
Validation	All primary anti-SARS-2 CoV-2-S mAbs were validated using purified SARS-CoV-2 RBD or S proteins using ELISA or BLI assays. All secondary antibodies were validated by each respective manufacturer per their associated DataSheets.

Eukaryotic cell lines

Policy information about cell lines

Cell line source(s)	Vero E6 (CRL-1586, American Type Culture Collection (ATCC), Vero-TMPRSS2, Diamond laboratory; Vero-hACE2-TMPRSS2, Graham laboratory, VRC/NIH; Expi-CHO (ThermoFisher, A29127), 293T/17 (ATCC CRL-11268)
Authentication	These were obtained from ATCC or other academic laboratories and grew and performed as expected (or stained positively for antigens (TMPRSS2 and hACE2) by flow cytometry). No additional specific authentification was performed.
Mycoplasma contamination	All cell lines are routinely tested each month and were negative for mycoplasma.

Commonly misidentified lines (See ICLAC register)	This study did not involve any commonly misidentified cell lines.

Animals and other organisms

Policy information about studies involving animals; ARRIVE guidelines recommended for reporting animal research

Laboratory animals	BALB/c mice (both sexes, 4 months); Syrian Golden hamsters (both sexes, 1 year), Rhesus macaques (male 4 years): these were used in previous studies. In this study, only banked sera was used
Wild animals	N/A
Field-collected samples	N/A
Ethics oversight	All experiments were conducted with approval of the Institutional Animal Care and Use Committee at the Washington University School of Medicine (Assurance number A3381-01) - [prior studies, as current one did not have active animal work]

Note that full information on the approval of the study protocol must also be provided in the manuscript.

Human research participants

Policy information about studies involving human research participants

Population characteristics	The convalescent patients were recruited from the St. Louis metropolitan area who experienced mild SARS-CoV-2 infection. None of those patients required intubation. Human subjects information: (a) Convalescent subjects: Median age = 50 (21-69); Gender = Females (57%); Race = White (95%); (b) Vaccinated subjects: Median age = 45 (26-64); Gender = Females (64%); Race = White (94%).
Recruitment	Convalescent plasma donors were recruited from the St. Louis metropolitan area by the Washington University Infectious Diseases Clinical Trials Unit. Vaccinated individuals were health care workers at Washington University School of Medicine and Barnes and Jewish hospital. Potential self-selection and recruiting biases are unlikely to affect the parameters we measured.
Ethics oversight	Washington University School of Medicine Institutional Review Board. IRB approval numbers: 202003186 (WU353), 202012081 (WU368) and 202012084 (COVaRiPAD)

Note that full information on the approval of the study protocol must also be provided in the manuscript.

Flow Cytometry

Plots

Confirm that:

☒ The axis labels state the marker and fluorochrome used (e.g. CD4-FITC).

☒ The axis scales are clearly visible. Include numbers along axes only for bottom left plot of group (a 'group' is an analysis of identical markers).

☒ All plots are contour plots with outliers or pseudocolor plots.

☒ A numerical value for number of cells or percentage (with statistics) is provided.

Methodology

Sample preparation	Expi-CHO cells were transiently transfected with SARS-CoV-2-S expression vectors. Two days later, intact cells were collected for immunostaining with mAbs.
Instrument	ZE5 Cell Analyzer (Biorard)
Software	FlowJo software (v9, TreeStar)
Cell population abundance	N/A
Gating strategy	Gating on live cells was performed using FSC and SSC

☒ Tick this box to confirm that a figure exemplifying the gating strategy is provided in the Supplementary Information.